Skin Cancer: The Primary Tumors

9

Ximena Wortsman, Laura Carreño, and Claudia Morales

How to deal and what to look for in the primary lesion

Contents

9.1 Introduction

Skin cancer is the most common form of cancer in human beings, therefore a frequent cause of dermatological consultation. Cutaneous cancer can be categorized into two main types: non-melanoma skin cancer (NMSC) and melanoma. NMSC constitutes up to 95 % of skin malignancies, and melanoma up to 5 %. The most frequent forms of presentations of NMSC are basal cell carcinoma (BCC) and squamous cell carcinoma (SCC) [1].

Less common skin malignancies are dermatofibrosarcoma protuberans, angiosarcoma, Merkel's cell carcinoma, Kaposi's sarcoma, and cutaneous lymphomas.

The goal of this chapter is to review the sonographic patterns of the most common forms of skin cancer and the role of sonography in the evaluation of these entities.

9.2 Non-Melanoma Skin Cancer

NMSC (BCC and SCC) is most frequent on areas exposed to the sun, and can be associated with functional and cosmetic problems that can complicate the evolution and prognosis in highly exposed areas of the body. Thus, NMSC presents frequently in facial locations that include the skin of the eyelids, nose, lips, and ears where the cutaneous layers are thin and involvement of cartilage and orbicular muscles may easily occur. Recurrences and multiple locations are not uncommon and can make the management of patients even more difficult. Incomplete excision of primary NMSC lesions has been reported in up to 45.5 % of cases [2].

X. Wortsman, MD (✉)
Department of Radiology and Dermatology,
Institute for Diagnostic Imaging and
Research of the Skin and Soft Tissues,
Clinica Servet, University of Chile, Faculty of Medicine,
Almirante Pastene 150, Providencia, Santiago, Chile
e-mail: xwo@tie.cl, xworts@yahoo.com, www.sonoskin.com

L. Carreño, MD • C. Morales, MD
Department of Pathology, Dermopathology Section,
Hospital Clinico Universidad de Chile, Faculty of Medicine,
University of Chile, Santiago, Chile
e-mail: lcarrenotoro@gmail.com; claudiamohuber@gmail.com

X. Wortsman, G.B.E. Jemec (eds.), *Dermatologic Ultrasound with Clinical and Histologic Correlations*,
DOI 10.1007/978-1-4614-7184-4_9,

9.2.1 Basal Cell Carcinoma

BCC, also called epithelioma, is the most frequent form of cancer among human beings and composes 75–95 % of all skin cancers. It is rarely fatal but could be highly disfiguring [1–3]. Clinically, BCC appears as a slow-growing, painless, erythematous, pearly papule or nodule that usually easily bleeds after minor trauma or may ulcerate (rodent ulcer). These tumors can also mimic a scar on physical examination.

Greater than 70 % of BCC tumors are located on the face, and the most frequent locations are the nose and eyelids [2, 3]. This type of skin cancer rarely metastasizes, although in areas where the skin is thin, there is a significant risk of involvement of deeper layers such as muscle, cartilage, or bone.

BCCs can be separated into several subtypes: superficial or in situ multifocal (15–35 %); diffuse or infiltrative that include morpheaform and micronodular subtypes (4–17 %); nodular, that also include nodulocystic, adenoid, and ulcerative subtypes (45–60 %); and pigmented (1–7 %). There are also other less common histological variants of BCC such as pleomorphic, clear cell, signet ring, granular, infundibulocystic, metaplastic, and keloidal subtypes, among others. Additionally, the different categories can be mixed within the same lesion or the patient may present multiple lesions with more than one subtype. Histologically, BCC is composed of a fibrous stroma and islands of basaloid cells that are dependent cells similar to the basal cells of the epidermis and hair follicles. The cells show indistinct cytoplasmic borders and oval basophilic vesicular nuclei. The nodulocystic subtype shows cysts with abundant mucin and the adenoid variant presents a pseudoglandular appearance. The morpheaform subtype shows narrow epithelial strands compressed by dense fibrous stroma and hyalinization [4] (Figs. 9.1, 9.2, 9.3, 9.4, 9.5, 9.6, and 9.7).

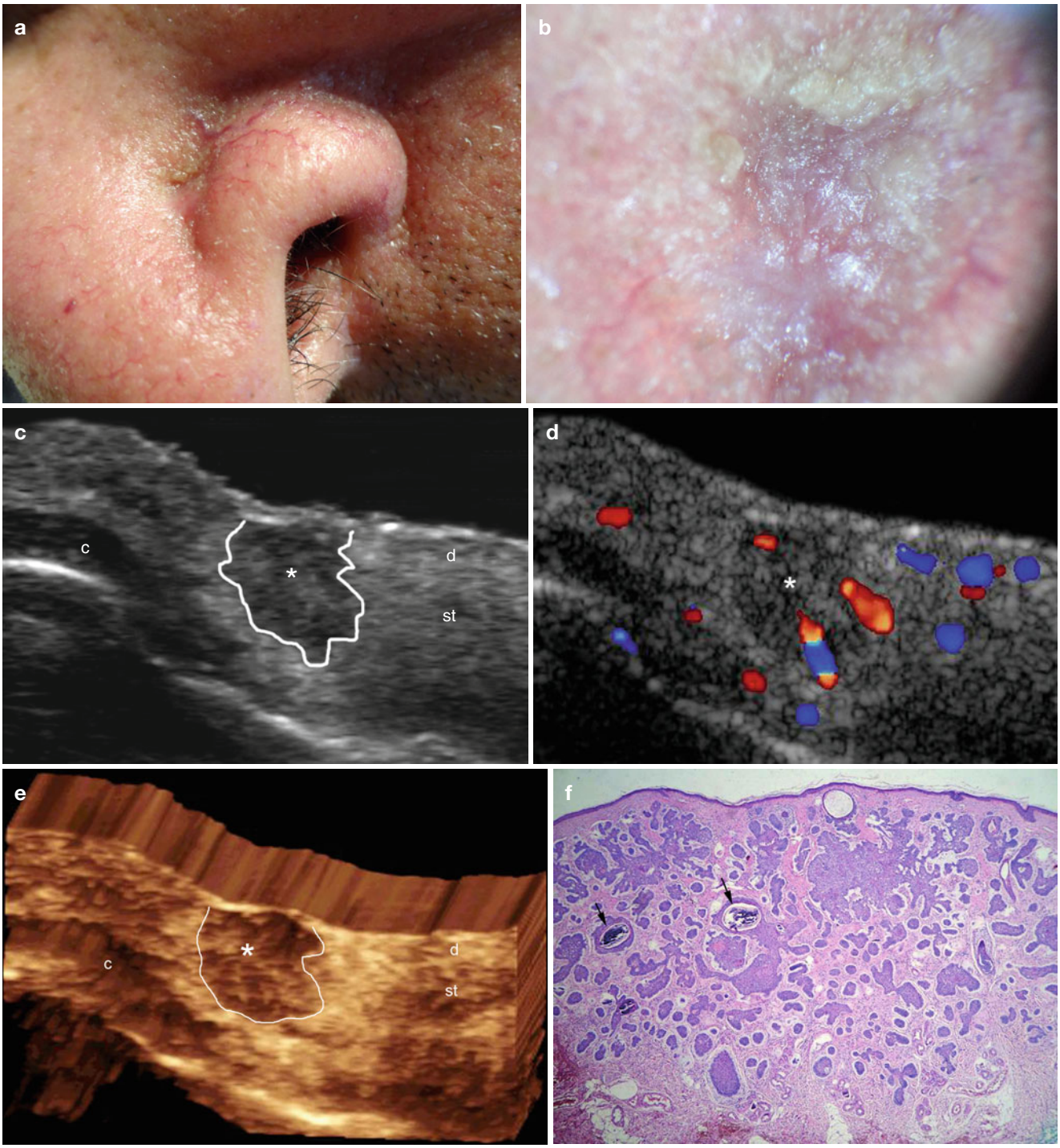

Fig. 9.1 (**a**–**f**) Basal cell carcinoma. (**a**, **b**) Clinical images (**a** photograph and **b** dermoscopy) of a pearly and erythematous lesion in the left nasal wing. (**c**) Grey scale ultrasound image (transverse view) shows well-defined hypoechoic structure (*, outlined) with irregular borders located in the dermis and subcutaneous tissue. The left nasal cartilage is unremarkable. (**d**) Color Doppler ultrasound image (transverse view) demonstrates increased blood flow in the lesional area. (**e**) The lesion shown in 3D (5–8 s sweep, transverse view). (**f**) Histology (HE × 40 zoom) shows small and large nests of basaloid cells suggestive of macro- and micronodular basal cell carcinoma. Calcium deposits (*arrows*) are also detected. *Abbreviations*: *d* dermis, *st* subcutaneous tissue, *c* nasal cartilage

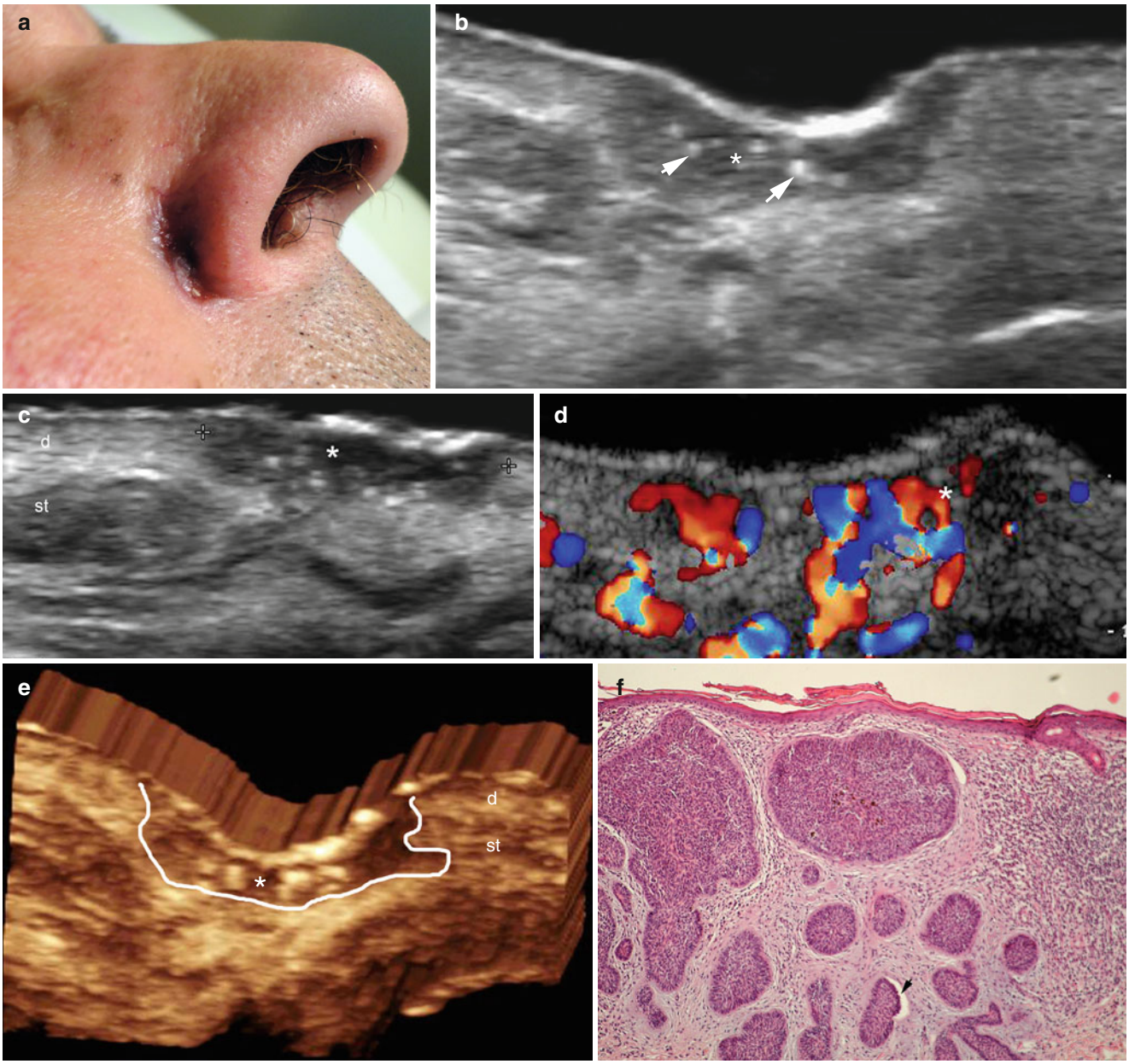

Fig. 9.2 (**a**–**f**) Basal cell carcinoma. (**a**) Clinical photograph shows a reddish swelling in the right nasofold line. (**b**, **c**) Grey scale ultrasound images (**b** transverse and **c** longitudinal views) demonstrate a well-defined oval-shaped hypoechoic lesion (*) located in the dermis and upper subcutaneous tissue. Notice the hyperechoic spots (*arrows*) within the structure. The right nasal cartilage is unremarkable. (**d**) Color Doppler ultrasound image (longitudinal view) shows increased blood flow within the lesion. (**e**) 3D reconstruction of the tumor (*, outlined; 5–8 s sweep, transverse view). (**f**) Histology (HE 100 × zoom): Macro- and micronodular infiltrate of basaloid cells with a palisade arrangement. A cleft is noted surrounding a cell nest. Fibrous stroma and inflammatory cells are also detected. *Abbreviations*: *d*, dermis; *st*, subcutaneous tissue

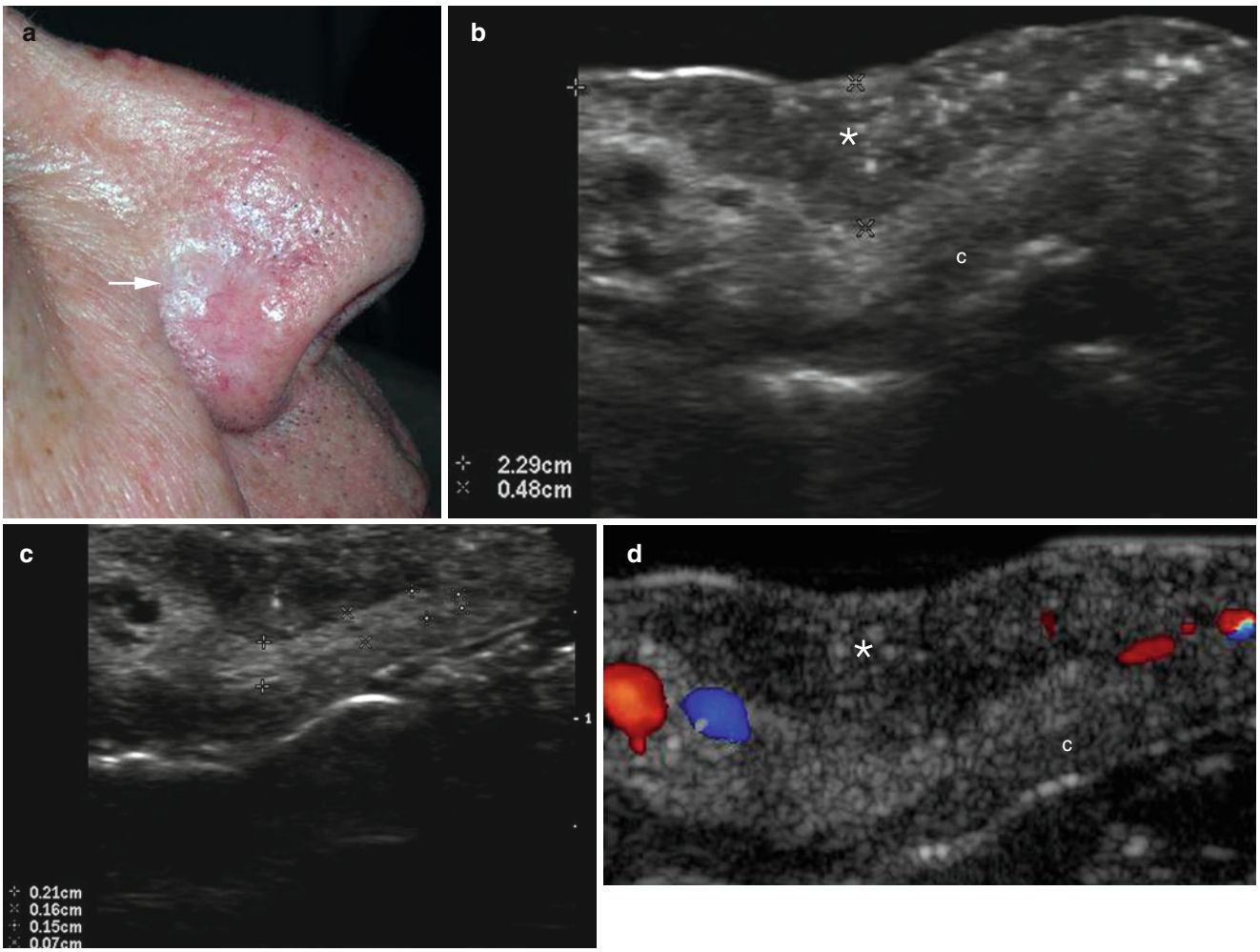

Fig. 9.3 (**a**–**g**) Morpheaform basal cell carcinoma. (**a**) Clinical image shows a pearly and erythematous nodule (*arrow*) in the right nasal wing. (**b**, **c**) Grey scale ultrasound images (transverse views; **b** superficial and **c** deep focus) demonstrate a 2.29 × 0.48 cm well-defined fusiform hypoechoic lesion located in the dermis and upper subcutaneous tissue. Notice the multiple hyperechoic spots within the lesion and the tapering of the distance (0.21–0.07 cm going from the posterior to anterior aspect) between the tumor and the right nasal cartilage (**c**). The right nasal cartilage is unremarkable. (**d**) Grey scale ultrasound image demonstrates a small vessel within the lesion (*). (**e**) The surgical defect (Mohs's surgery). (**f**) The lesion after surgical reconstruction. (**g**) Histology (HE × 100 zoom): cords and angular nests of atypical basaloid cells (*arrows*). (Figs. **a**, **e**, and **f** are courtesy of Dr. Daniela Saavedra) *Abbreviations*: *d* dermis, *st* subcutaneous tissue, *c* nasal cartilage.

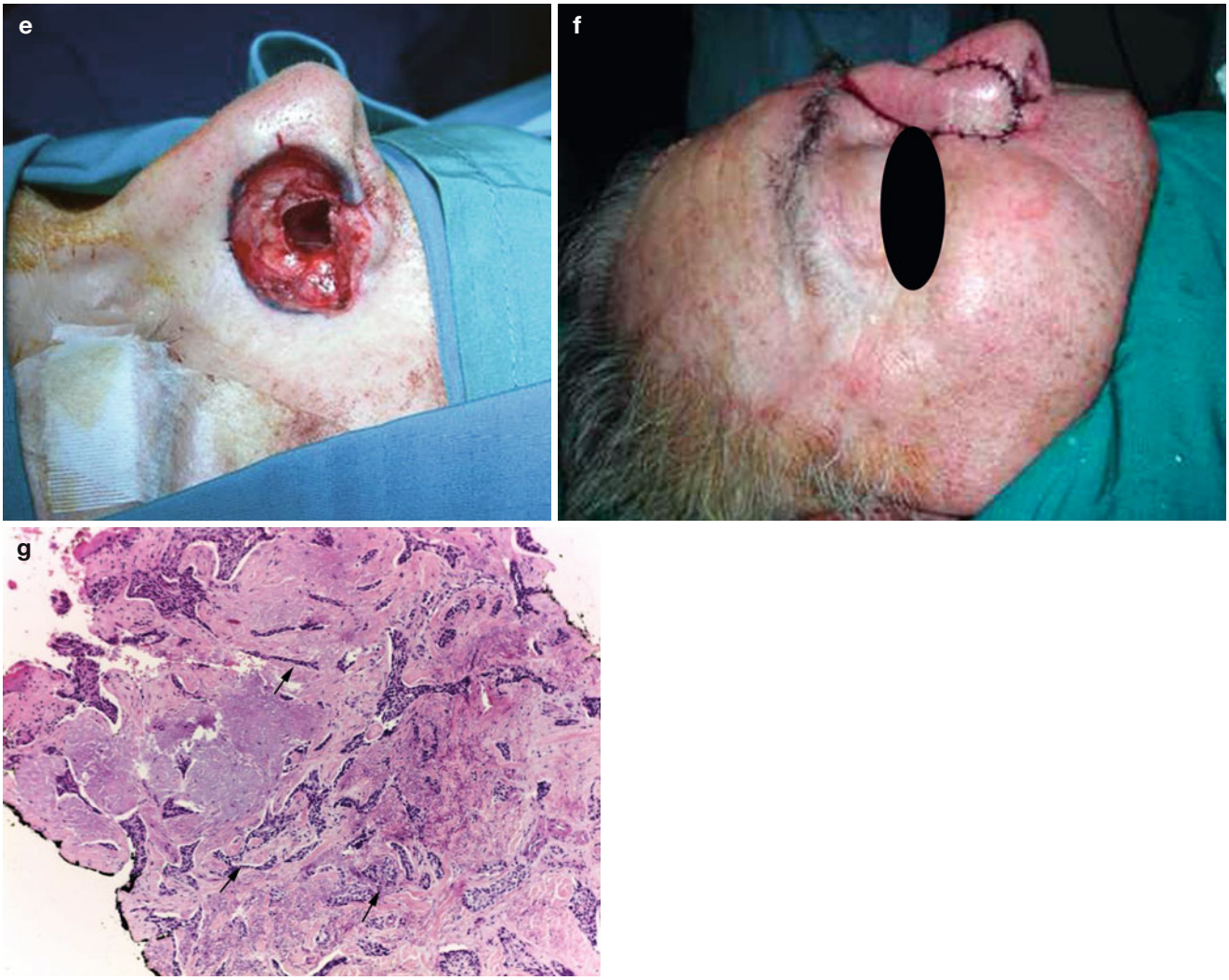

Fig. 9.3 (continued)

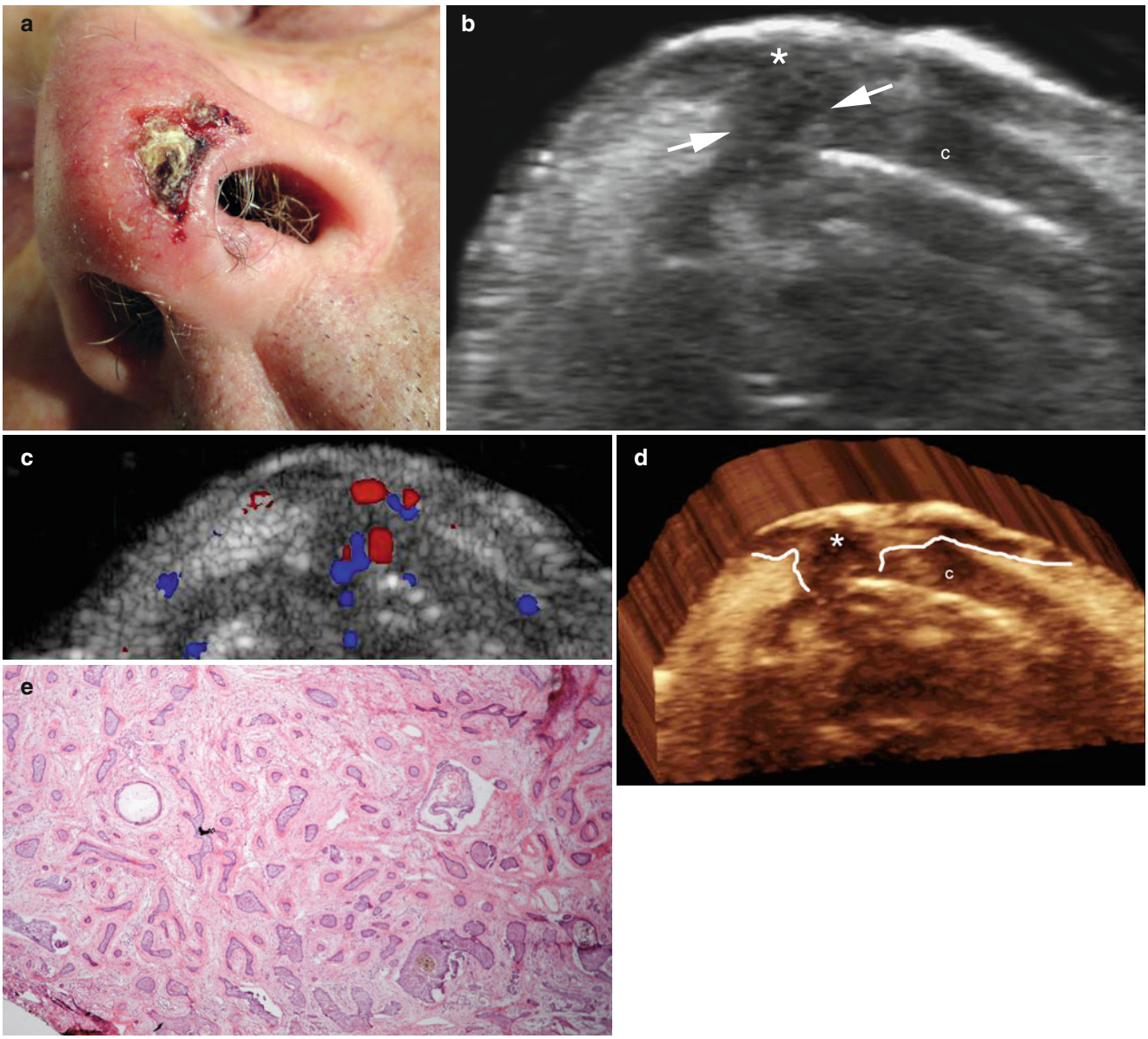

Fig. 9.4 (**a**–**e**) Basal cell carcinoma with involvement of the nasal cartilage. (**a**) Clinical photograph shows ulcerated erythematous lesion in the left nasal wing. (**b**) Grey scale ultrasound image (transverse view) demonstrates hypoechoic solid lesion (*) that involves the anterior aspect (*arrows*) of the left nasal cartilage. (**c**) Color Doppler ultrasound image (transverse view) shows increased vascularity in the lesional area including the nasal cartilage. (**d**) 3D view of the tumor (*, transverse view, outlined, 5–8 s sweep). (**e**) Histology (HE ×40 zoom): dermis with nests of atypical basaloid cells of variable sizes and shape. The small size nests predominate within the tumor that is surrounded by a fibrous stroma. *Abbreviations*: *d* dermis, *st* subcutaneous tissue, *c* cartilage

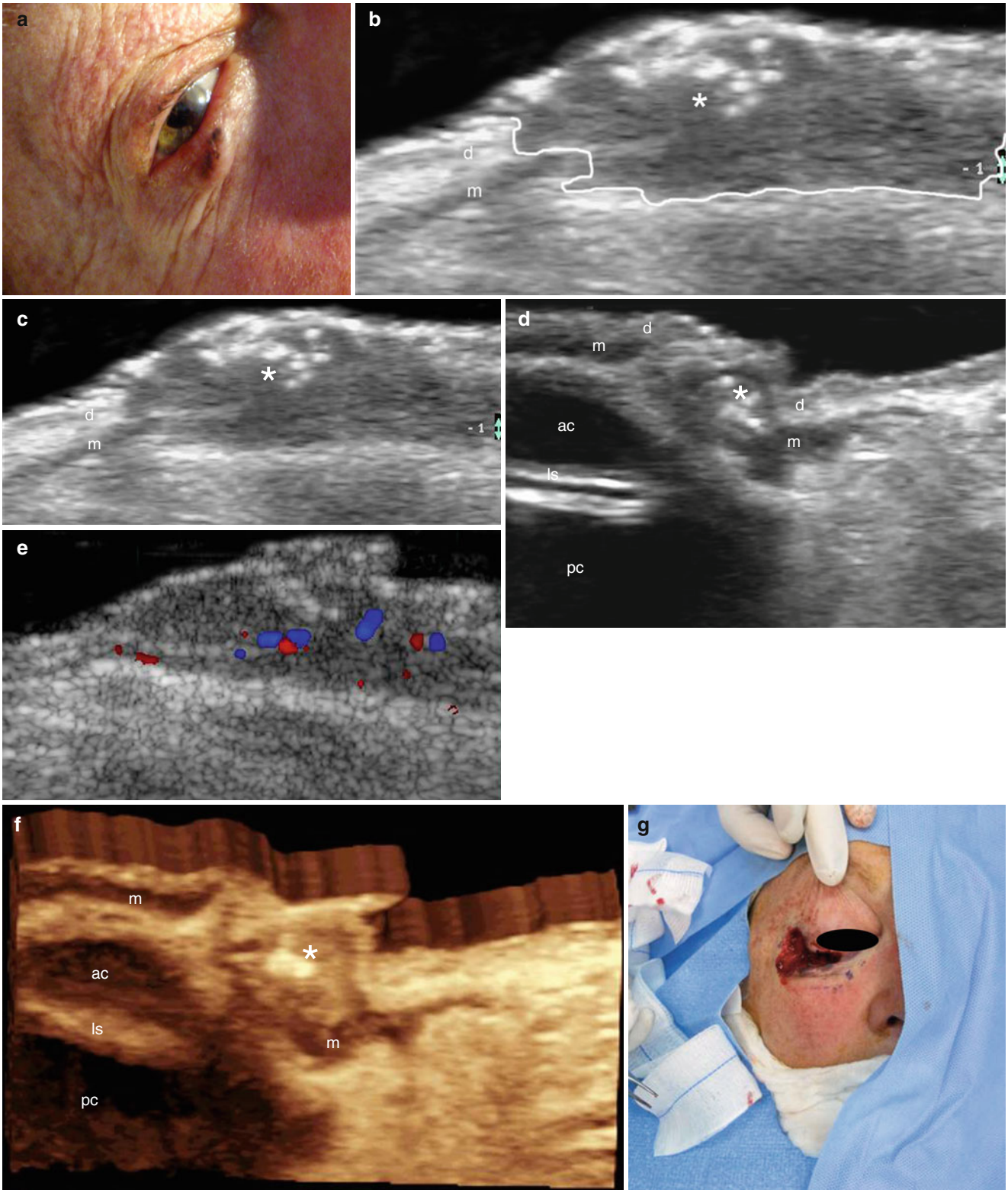

Fig. 9.5 (**a**–**g**) Basal cell carcinoma with involvement of the orbicular muscle of the lower eyelid. (**a**) Clinical photograph shows a pigmented and erythematous lump in the right lower eyelid. (**b**–**d**).Grey scale ultrasound images (**b** and **c** transverse views; **d** longitudinal view) demonstrated ill-defined hypoechoic lesion (*) that involves the dermis and the underlying orbicularis muscle. The tumor presents irregular borders that are outlined in figure (**b**). Notice the hyperechoic spots within the tumor. (**e**) Color Doppler ultrasound image (transverse view) shows increased vascularity within the lesional area. (**f**) 3D reconstruction of the tumor (longitudinal view; 5–8 s sweep). (**g**) The surgical excision of the tumor (Mohs's surgery). Images **a** and **g** are courtesy of Dr. Daniela Saavedra. *Abbreviations*: *d* dermis, *m* orbicularis muscle of the eyelid, *ac* anterior chamber of the ocular globe, *pc* posterior chamber of the ocular globe, *l* lens

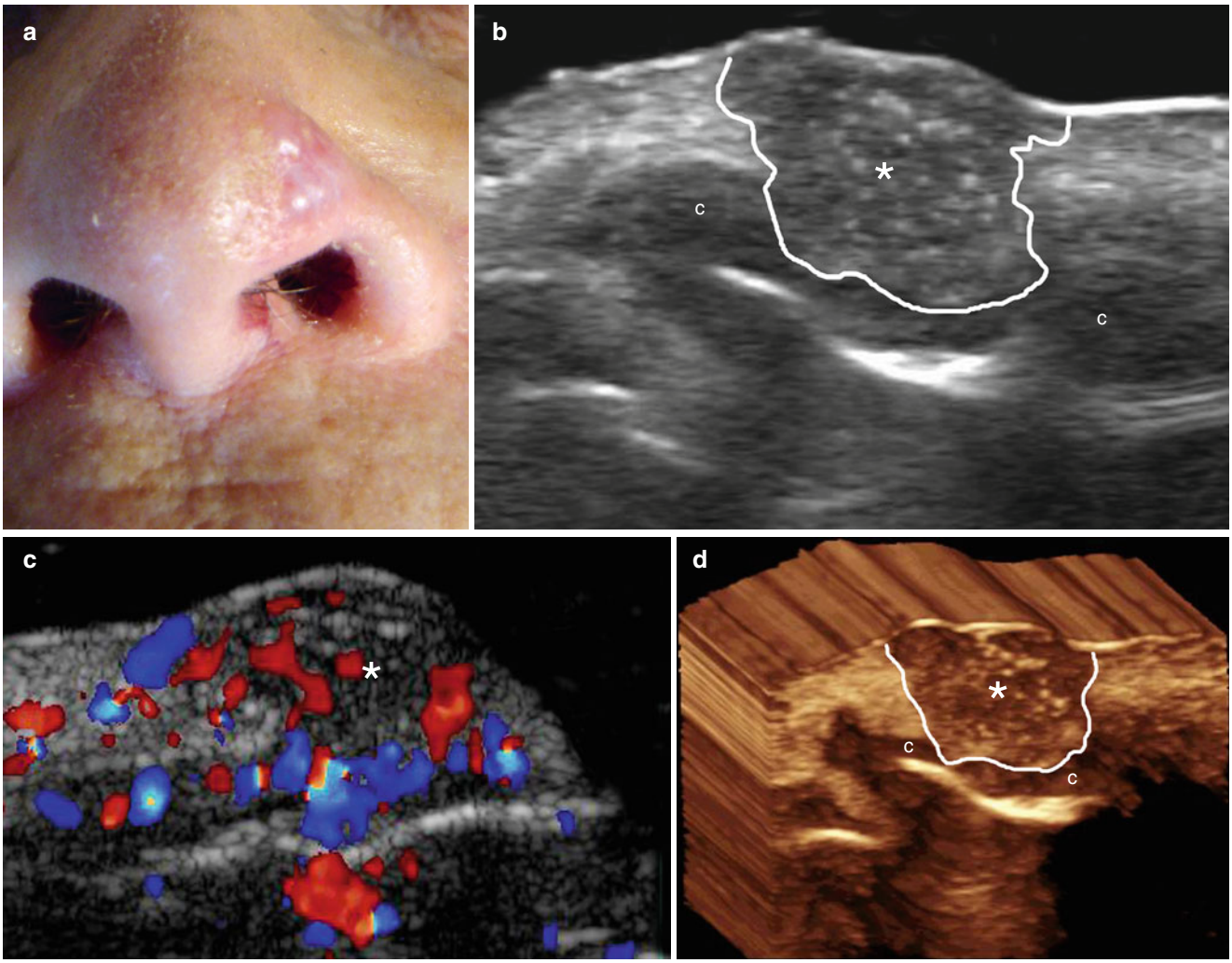

Fig. 9.6 (**a**–**d**) Basal cell carcinoma with involvement of the left nasal cartilage. (**a**) Clinical photograph shows pearly erythematous swelling in the left nasal wing. (**b**) Grey scale ultrasound image (transverse view) demonstrates well-defined hypoechoic solid lesion (*) with irregular borders (outlined) that involves the skin layers and the underlying nasal cartilage. Notice the hyperechoic spots within the tumor. (**c**) Color Doppler ultrasound image (longitudinal view) shows increased vascularity in the lesional area (*). (**d**) 3D reconstruction of the tumor (*, outlined). *Abbreviation*: *c* nasal cartilage

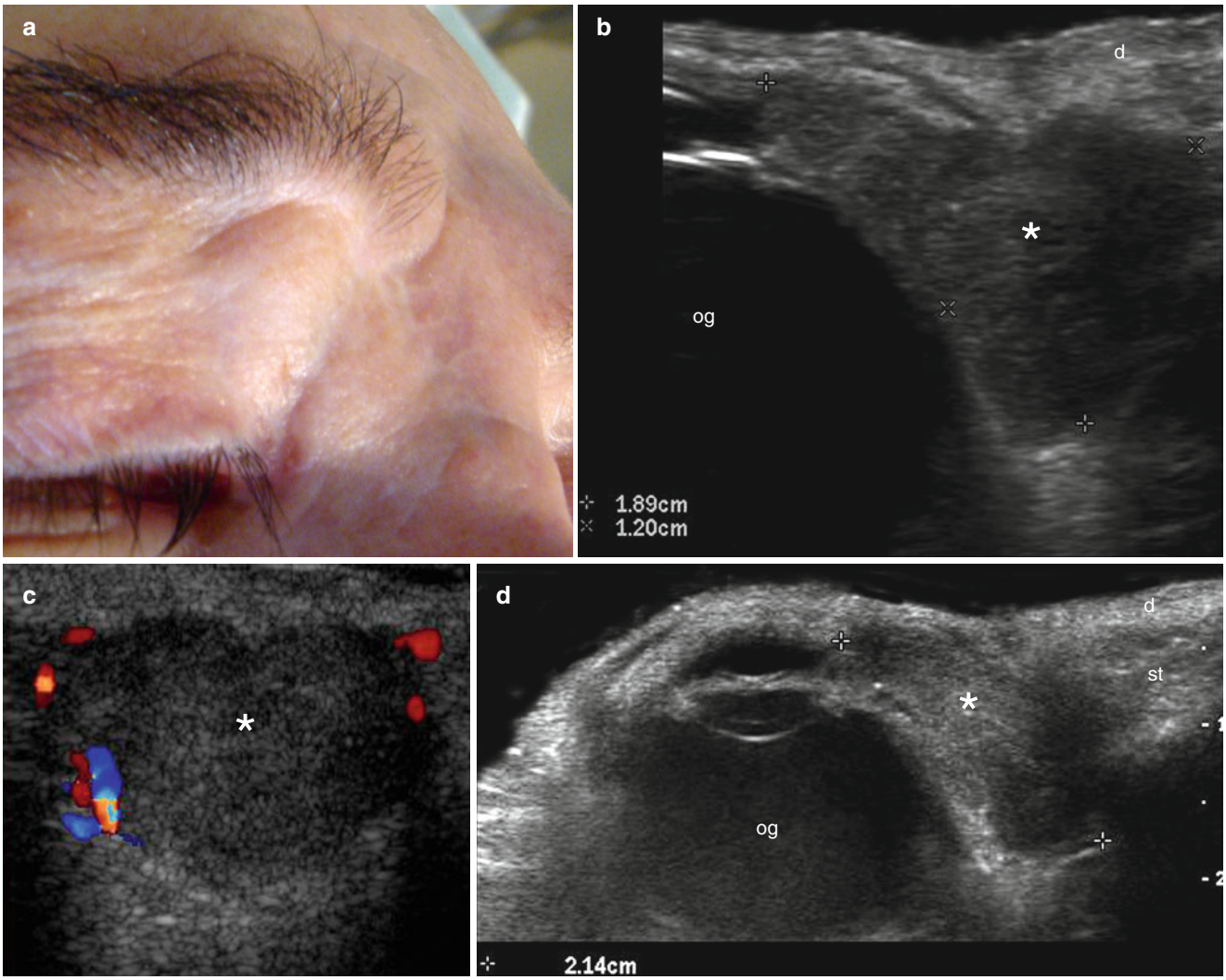

Fig. 9.7 (**a**–**d**) Recurrent basal cell carcinoma. (**a**) Clinical photograph shows skin-colored swelling in the medial aspect of the right upper eyelid. (**b**) Grey scale ultrasound image (transverse view) demonstrates 1.89 × 1.20 cm well-defined hypoechoic mass (*) that affects the subcutaneous tissue and extends into the medial aspect of the orbit. (**c**) Color Doppler ultrasound image (longitudinal view) shows increased vascularity in the periphery of the tumor. (**d**) Grey scale ultrasound image (extended field of transverse view) demonstrates a wide transverse extension of the tumor (*, 2.14 cm wide). *Abbreviations*: *d* dermis, *st* subcutaneous tissue, *og* ocular globe

9.2.2 Squamous Cell Carcinoma

Cutaneous SCC is the second most common skin cancer, accounting for 20% of all cutaneous malignancies. Most of the tumors are found on the head and neck skin, and cumulative ultraviolet exposure is believed to be the most likely etiological factor. Most deaths from SCC occur in a high-risk group of patients that is composed of tumors greater than 2 cm in diameter; tumor thickness over 4 mm; moderately/poorly differentiated or desmoplastic histological SCC subtype; ear, lip, hand, feet, or genital tumor site; perineural or lymphovascular invasion; nodal metastasis at presentation; recurrent SCC; SCC arising from scars or chronic skin disease, for example, chronic ulcers; and SCC arising in immunosuppressed patients [5]. Furthermore, thickness (or depth of invasion) is an important predictor of metastases in SCC [6]. Thus, ultrasound may support identification of the high-risk SCC group that is associated with a greater mortality and morbidity.

Additionally, there are SCC-related lesions: Bowen's disease, the in situ form of SCC, and actinic keratosis, a precancerous skin lesion that usually appears in photodamaged skin that potentially can become a squamous cell cancer.

SCC presents clinically as a slow-growing usually painless, indurated lesion with a rough, scaly, erythematous surface that easily bleeds and can be nodular, ulcerated, plaque-like, or verrucous. The ulceration can present with a necrotic center and a prominent rim. Common locations are the lips, ear pinna, scalp, and dorsal aspect of the hands. Hence, infiltration of the deeper layers and metastasis is more frequent with SCC. Metastasis can occur to the regional lymph nodes and also to the liver, bones, lungs, and brain.

Histologically, SCC presents as infiltrating sheets and islands of variably differentiated squamous epithelium and a variable degree of mitotic activity (pleomorphism). Keratocysts and keratin pearls may also be found, with neurotropism and lymphovascular invasion providing poor prognosis. There are variants of SCC such as clear cell SCC, spindle cell, desmoplastic acantholytic, pseudovascular or pseudoangiosarcomatous, adenosquamous, mucoepidermoid, and verrucous [7] (Figs. 9.8, 9.9, 9.10, 9.11, and 9.12)

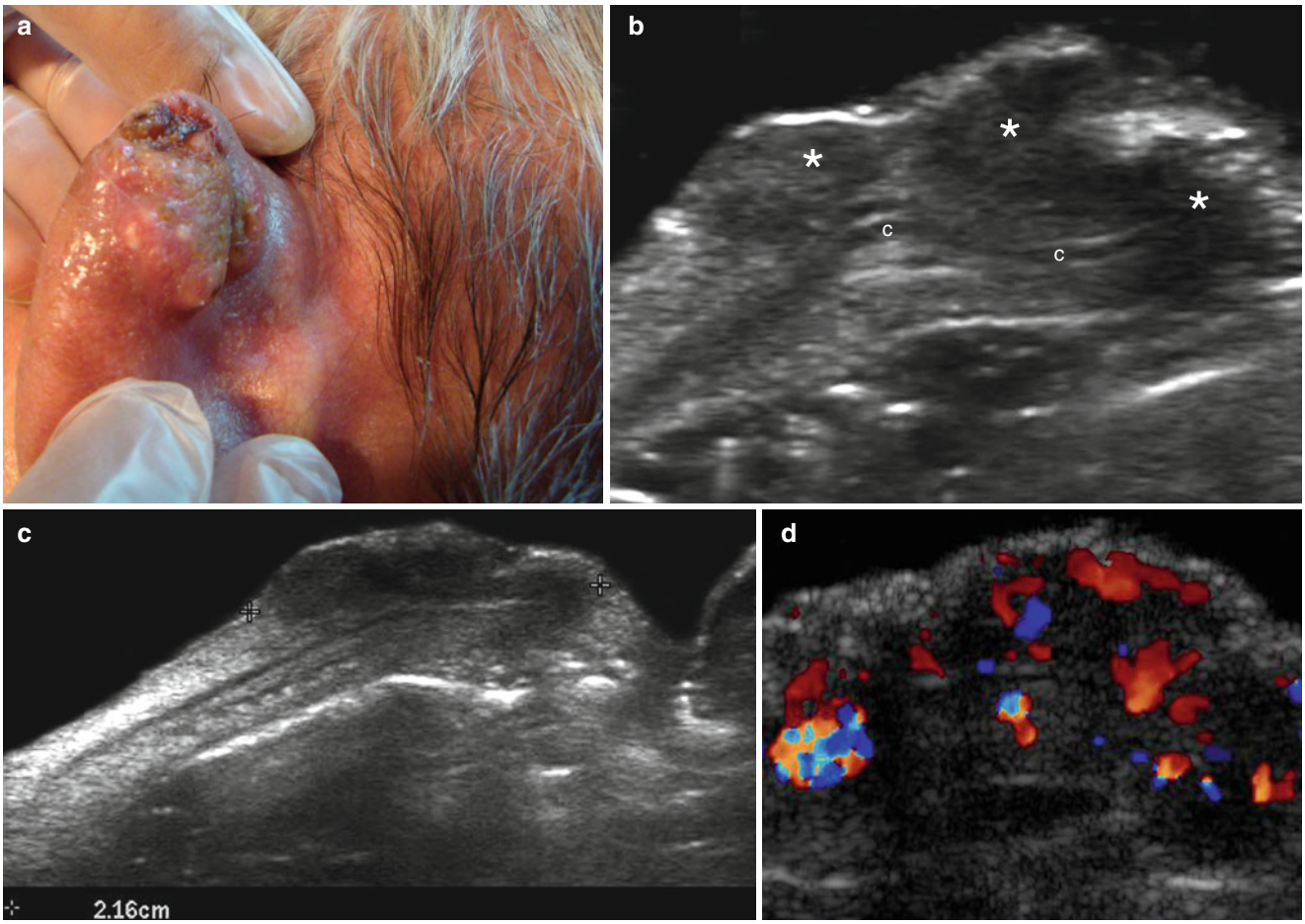

Fig. 9.8 (**a**–**d**) Squamous cell carcinoma. (**a**). Clinical photograph shows ulcerated erythematous swelling in the left ear pinna. (**b**, **c**) Grey scale ultrasound images (transverse views from the posterior aspect of the ear pinna; **b** zoomed image; **c** extended field of view) shows hypoechoic mass (*) that presents irregular borders and involves the posterior and anterior skin layers. The lesion embraces the ear cartilage and measures 2.16 cm in transverse axis. (**d**) Color Doppler ultrasound image (transverse view) demonstrates increased vascularity within the lesion. *Abbreviation*: *c* cartilage

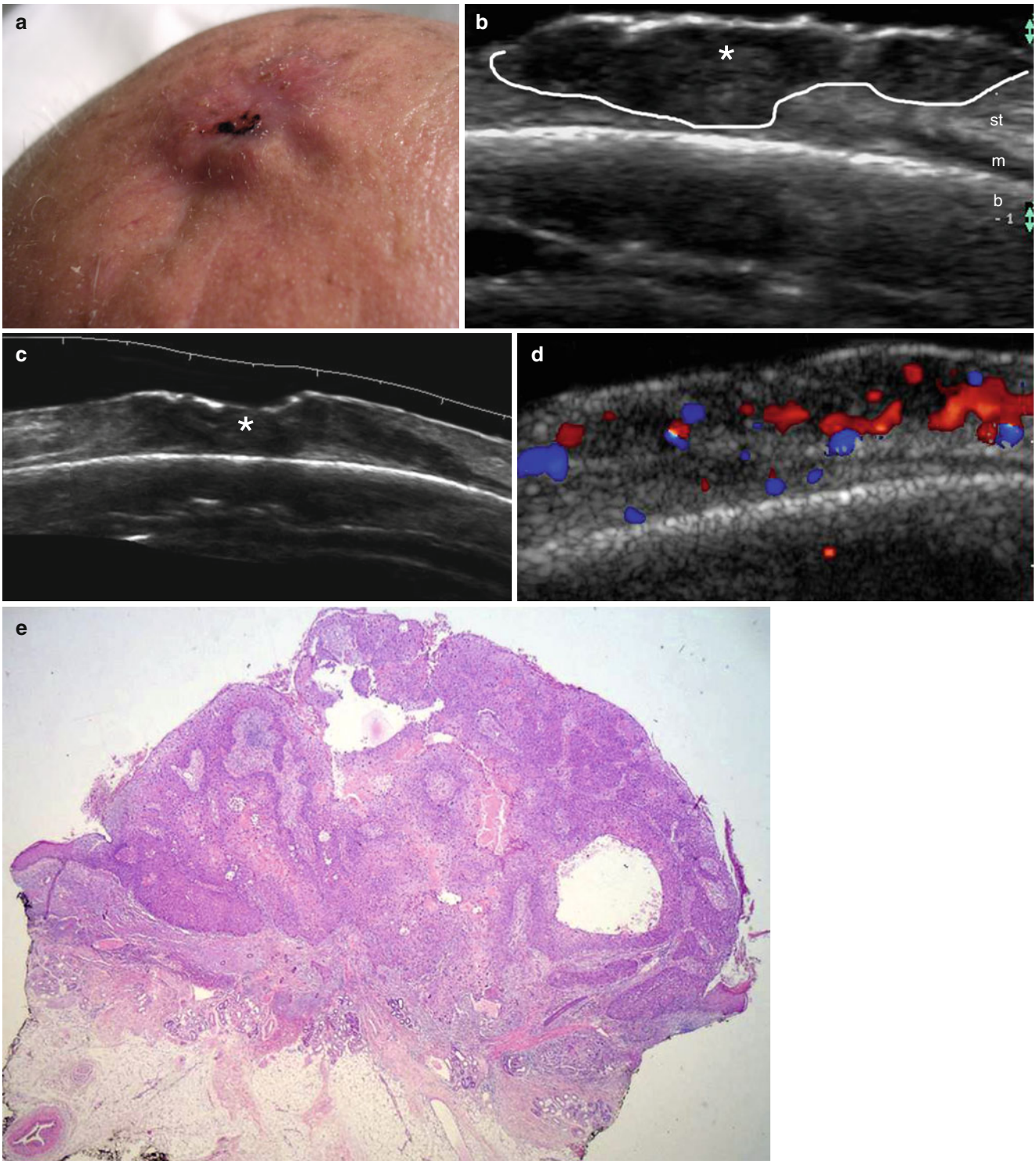

Fig. 9.9 (**a**–**e**) Squamous cell carcinoma. (**a**) Clinical photograph shows ulcerated erythematous swelling in the scalp. (**b**, **c**) Grey scale ultrasound images (**b** zoomed image and **c** extended field of view) demonstrate hypoechoic solid lesion (*, outlined) that involves the epidermis, dermis, subcutaneous tissue, and part of the epicranius muscle. The bony margin of the skull is unremarkable. (**d**) Color Doppler ultrasound image (transverse view) shows increased blood flow in the lesional area. (**e**) Histology (HE 40× zoom): neoplastic proliferation of atypical squamous cells with irregular disposition. *Abbreviations*: *st* subcutaneous tissue, *m* epicranius muscle, *b* bony margin of the skull

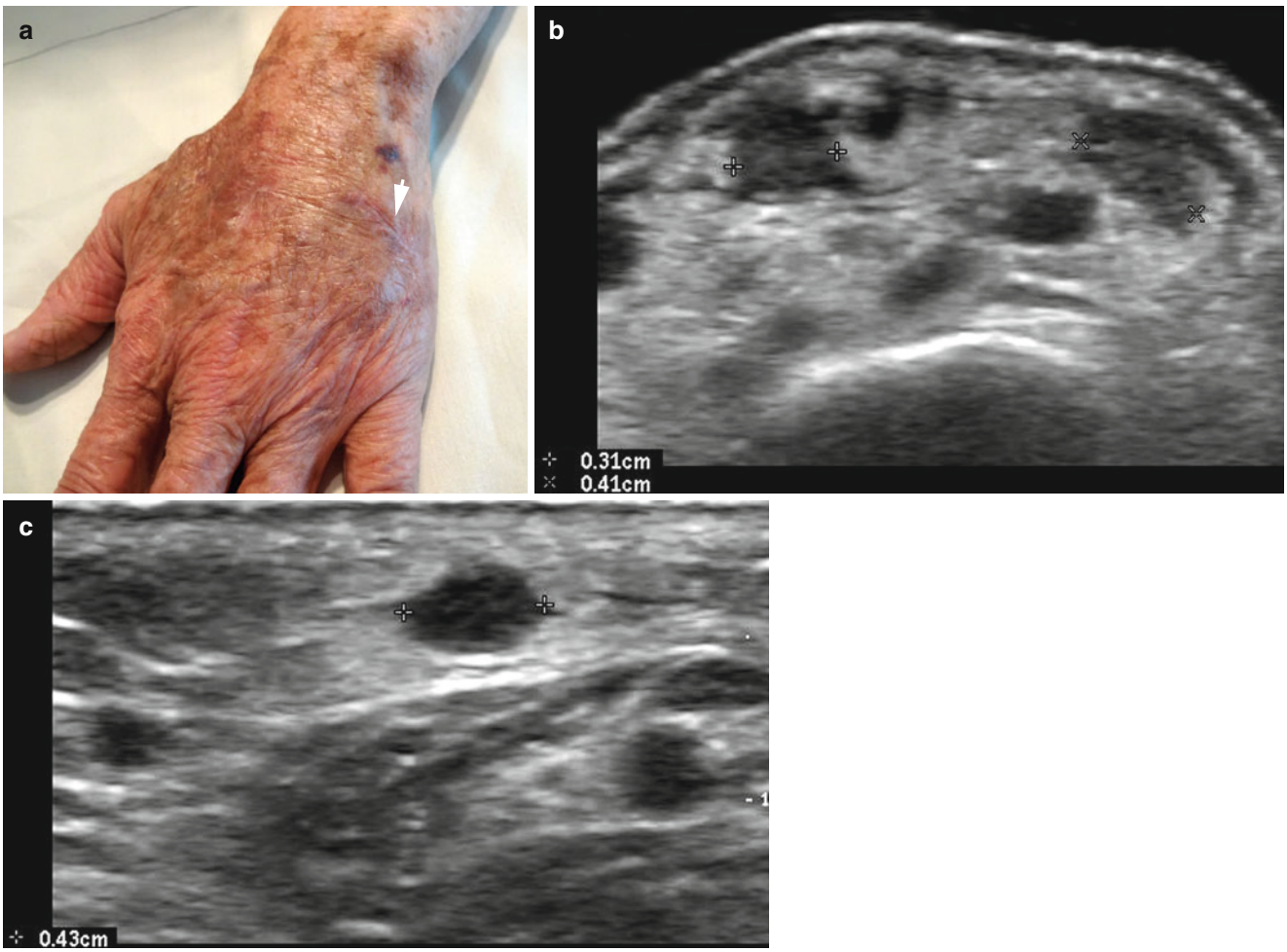

Fig. 9.10 (**a**–**c**) Satellite lesions in recurrent squamous cell carcinoma (SCC). (**a**) Clinical photograph shows an erythematous scar (*arrow*) in the dorsum of the left hand. The patient presented with a history of removal of an SCC lesion 6 months prior. (**b**, **c**) Grey scale ultrasound images (**b** transverse view located 0.5 cm proximal to the scar and **c** longitudinal view 0.5 distal to the scar level) show three well-defined hypoechoic nodules (between markers) located in the subcutaneous tissue that range in size between 0.3 and 0.43 cm. Increased echogenicity of the surrounding subcutaneous tissue is also detected

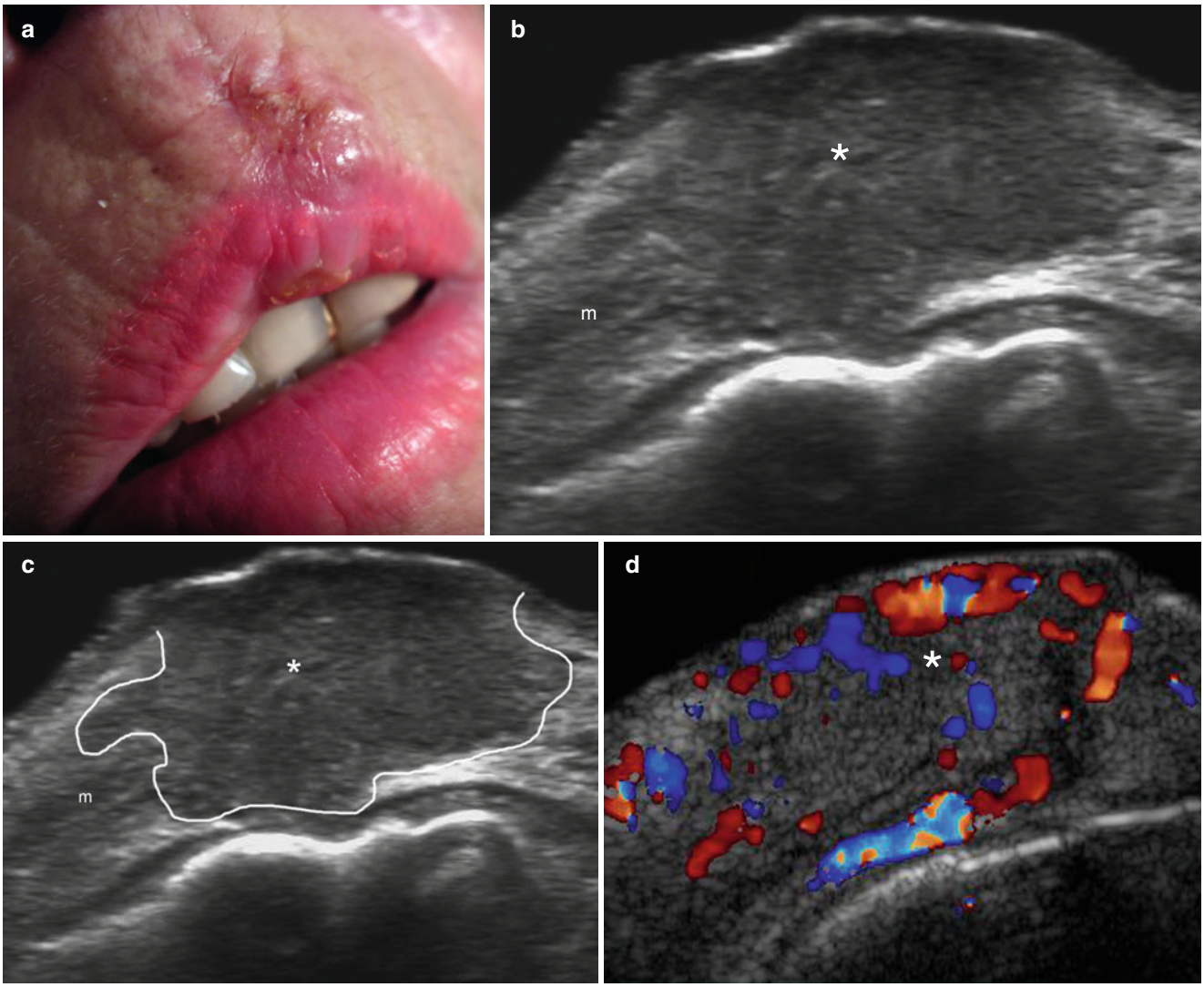

Fig. 9.11 (**a**–**d**) Recurrent squamous cell carcinoma (SCC) that involves the orbicularis muscle of the upper lip. (**a**) Clinical photograph shows erythematous swelling in the scar area. The patient has a history of removal of an SCC lesion 1 year prior in the same region. (**b**, **c**) Grey scale ultrasound images (transverse views; **c** the tumor is outlined) show a hypoechoic solid mass (*) that involves the skin layers and the orbicularis muscle of the upper lip. The tumor also bulges into the vestibular aspect of the lip. (**d**) Color Doppler ultrasound image (longitudinal view) demonstrates increased blood flow within the lesional region (*). *Abbreviation*: *m* orbicularis muscle of the lip

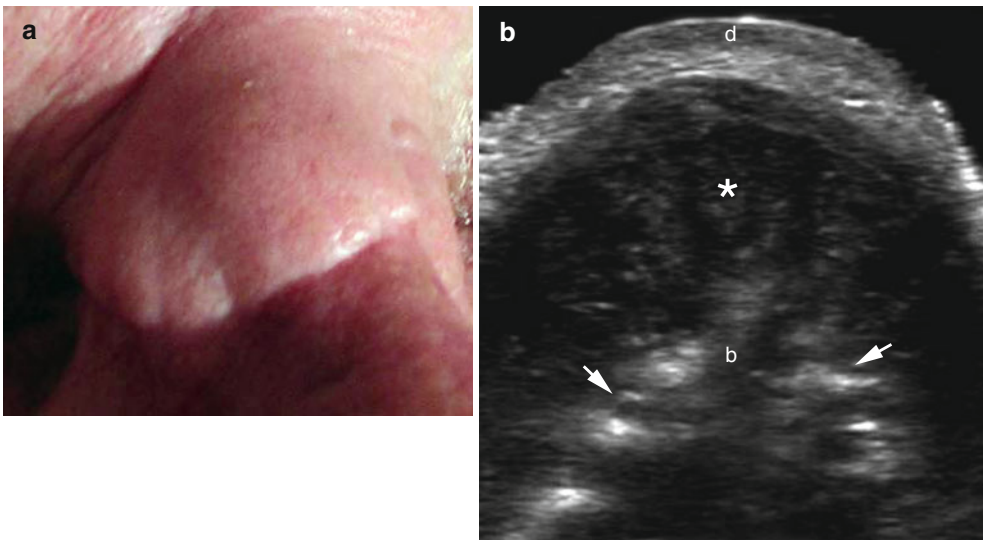

Fig. 9.12 (**a**–**b**) Recurrent squamous cell carcinoma (SCC) with involvement of the bony margin of the nasal bones. (**a**) Clinical image shows skin-colored swelling in the dorsum of the nose. The patient presented with a history of removal of an SCC lesion 3 years prior. (**b**) Grey scale image (transverse view) demonstrates a hypoechoic solid mass (*) that involves the subcutaneous tissue and the bony margin of the nasal bones (*arrows*). Notice the erosion of the bony margin of the nasal bones (*arrows*). *Abbreviations*: *d* dermis, *b* bony margin of the nasal bones

9.2.3 Staging of NMSC

Current staging of NMSC is based on the clinical measure of the tumor size, depth, loco-regional lymph node involvement, and distant metastasis. Tumors measuring ≥2 cm on the lips, ear, eye, or nose present a poor prognosis.

Not formally included among high-risk NMSC lesions are the ones present in immunosuppressed patients who show a higher incidence of NMSC under long-term immunosuppressive therapy or conditions. Thus, renal transplantation is associated with an increased incidence of NMSC caused by immunosuppressive treatments, and under this context, NMSC exhibits more aggressive biological and clinical courses, with higher rates of recurrence and mortality than in the general population. In renal transplants, SCC represents the most frequent skin malignancy (64.1 %), followed by BCC (17.9 %), Bowen's disease (10.2 %), basosquamous carcinoma (5.1 %), and a rare case of invasive sebaceous carcinoma (2.6 %) according to some reports [8, 9]

SCC is the most severe complication and most common cause of death in patients with junctional and recessive dystrophic epidermolysis bullosa [10, 11].

The inclusion of the sonographic parameters (diameter in all axes, blood flow, presence of deeper layers involvement and satellite lesions) may support the clinical staging of NMSC providing valuable data that can match the anatomical involvement for each patient. The latter features may help to perform a one-time treatment, decreasing the possibility of recurrences and improving the cosmetic prognosis of the patient.

9.2.4 NMSC Sonographic Characteristics

NMSC usually presents as hypoechoic and heterogeneous cutaneous tumors with irregular borders. Hyperechoic spots are frequently detected within BCC tumors. Low flow arterial vessels are commonly detected in the lesion and its periphery. The vascularity in BCC is commonly prominent at the bottom of the tumor [12, 13]. Nevertheless, squamous carcinoma is more aggressive upon presentation, therefore, infiltration of the deeper structures and/or loco-regional lymph nodes should be ruled out on the ultrasound examinations. Vascularity in SCC is frequently more prominent compared with BCC and shows greater presence of vessels within the lesion.

Two sonographic artifacts have been reported in BCC lesions. The first is termed the "angles at the bottom" of the lesion, which is produced by inflammatory components that include dilated vessels and giant cells. The second is termed the "blurry tumor" which is generated by a large presence of hyperplastic sebaceous glands that are isoechogenic with the primary lesion and can decrease the definition of the borders of the tumor [12].

Tips for BCC
- Well defined
- Hypoechoic
- Hyperechoic spots within the tumor
- Increased vascularity at the bottom of the lesion

Tips for SCC
- Hypoechoic lesion with irregular borders
- Involvement of deeper layers
- Increased vascularity within the tumor

9.3 Primary Cutaneous Melanoma

Primary cutaneous melanoma is the most aggressive type of cutaneous malignancy and constitutes 4–11 % of all skin cancers comprising greater than 75 % of cutaneous cancer-related deaths and provoking greater than 8,000 deaths per year in the United States [14]. Recurrence has been reported in up to 35.9 % of the treated cases, and can be even higher (46.1 %) when the head and neck region is considered [15, 16]. Melanomas usually present clinically in 95 % of the cases as hyperpigmented macules or nodules that can show irregular borders and ulcerations. Approximately 5 % of melanomas lack pigment and are called amelanotic melanomas. Amelanotic melanomas contain few and/or deeper granules of melanin that are commonly not detected by the naked eye which can delay diagnosis.

The staging of melanoma is based on the Breslow classification that relies on the sequential tumor infiltration (depth) of the cutaneous layers detected by histology which considers the measurement of the microscopic invasion from the stratum granulosum of the epidermis to the deepest portion of the tumor (Table 9.1) [17]. Thus, knowledge of the thickness of the tumor will modify important decisions pertaining to the management of the tumor, such as the size of the excision, the performance of a sentinel node procedure, or the final prognosis of the patient.

On histology, melanomas appear as nests of atypical melanocytes with irregular nuclei, nuclear pleomorphism, prominent nucleoli, spindle or epitheliod cells, and marked mitotic activity. The level of invasion is graded according to the Clark classification (Table 9.1) and the depth of the invasion is assessed using the Breslow index (Table 9.2), which are important prognostic factors for melanoma [18].

On sonography, melanomas usually appear as well-defined, oval- or fusiform-shaped, homogeneous, hypoechoic lesions with smooth borders, increased acoustic transmission, and variable degrees of vascularity, even though they commonly show hypervascularity on color Doppler imaging [19–25]. Sonography has been proved useful for discriminating melanomas thicker and thinner than 1 mm which is relevant for deciding the performance of a sentinel node procedure that is indicated in melanomas that measure greater than 1 mm in thickness [26], the vessels are commonly located within the lesion and may also be tracked using contrast-enhanced ultrasound. Assessment of the vascularity, including the peak systolic velocity of the arterial vessels, may provide an idea of the angiogenic power of the tumor that can correlate with the metastatic potential [27–29]. In cases with ulcerations, the epidermis can show irregularities or discontinuities, and increased echogenicity in the subcutaneous tissue may also be found. Because melanomas can show asymmetry in their thickness, the sonographic measurements should be performed at the deepest point. In the vicinity of the primary lesion, satellite lesions (arising within 2 cm from the primary tumor) or in transit metastasis (arising greater than 2 cm from the primary tumor) can be detected [24, 29, 30]. These secondary lesions appear as hypoechoic oval- or round-shaped with smooth or lobulated contours, mild to moderate heterogenicity, and enhanced acoustic through transmission structures frequently located in the subcutaneous tissue and with variable degrees of vascularity [18, 24, 31]. Ultrasound has been reported to alter the management of patients by detecting impalpable metastasis and helping to differentiate between benign and malignant masses [16, 31]. Usually, there is increased vascularity within the metastases on color Doppler imaging, although the presence of internal vessels can show a variable appearance that can go from hypo- to hypervascular. Occasionally, these metastases can present an irregular appearance and anechogenicity and can be sonographically misdiagnosed as abscesses. This challenging anechoic appearance has been reported as related more to hypercellularity and not as a result of necrosis [32]. The balloon shape, nodular thickening of the cortex, and loss of hyperechogenicity of the medullae are signs of malignant infiltration in regard to nodal infiltration [24]. The use of lower frequency probes in bulky primary melanomas may help to reach to the bottom of the lesion and provide a better definition of the extension (Figs. 9.13, 9.14, 9.15, 9.16, and 9.17).

Table 9.1 Clark classification of the levels of invasion in melanoma

Level I: in situ melanoma
Level II: invasion of the papillary dermis by single cells or small nets
Level III: invasive tumor usually as an expansile nodule abutting on the reticular dermis
Level V: invasion of the subcutaneous fat

Table 9.2 Breslow classification of the depth of melanoma

Tumor depth (mm)	Approximate 5-year survival (%)
<1	95–100
1–2	80–96
2.1–4	60–75
>4	50

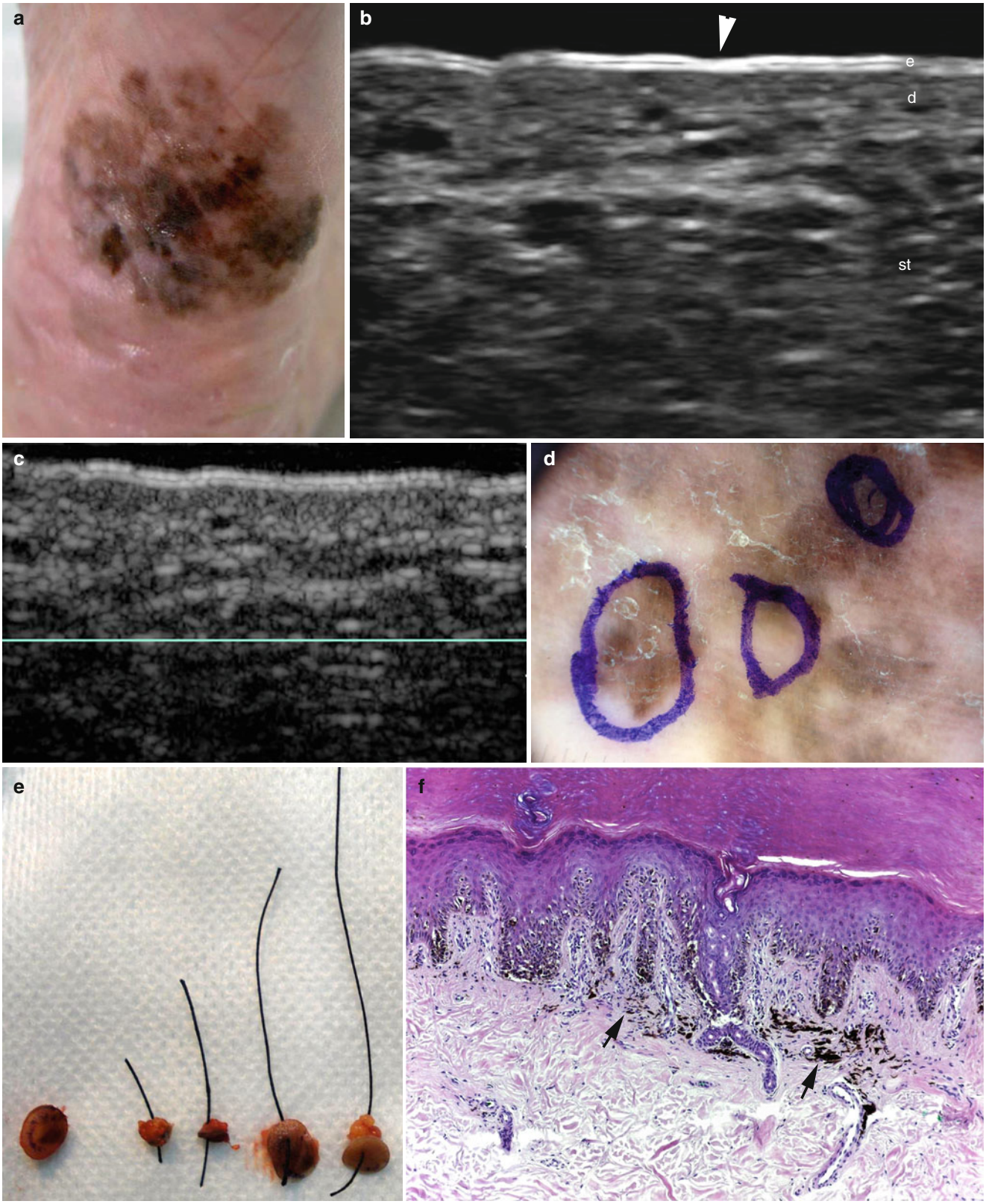

Fig. 9.13 (**a**–**f**) Melanoma in situ. (**a**) Clinical photograph shows hyperpigmented and irregular lesion in the sole of the left foot. (**b**) Grey scale ultrasound image (longitudinal view) demonstrates loss of the bilaminar pattern of the epidermis (*arrowhead*) in part of the lesion. Nevertheless, no sign of solid mass is detected. Notice the bilaminar appearance of the normal epidermis that is typically seen in the plantar region (glabrous skin). (**c**) Color Doppler ultrasound image (longitudinal view) shows no sign of regional hypervascularity. (**d**) Cutaneous marking of the biopsy sites. (**e**) Biopsy samples. (**f**) Histology (HE 40× zoom). Acral skin with atypical melanocytic proliferation in the dermo-epidermal junction. Deposition of melanin in the dermal melanophages. *Abbreviations*: *e* epidermis, *d* dermis, *st* subcutaneous tissue. (a, d, and e are courtesy of Drs. Veronica Catalan and Carlo Pezo)

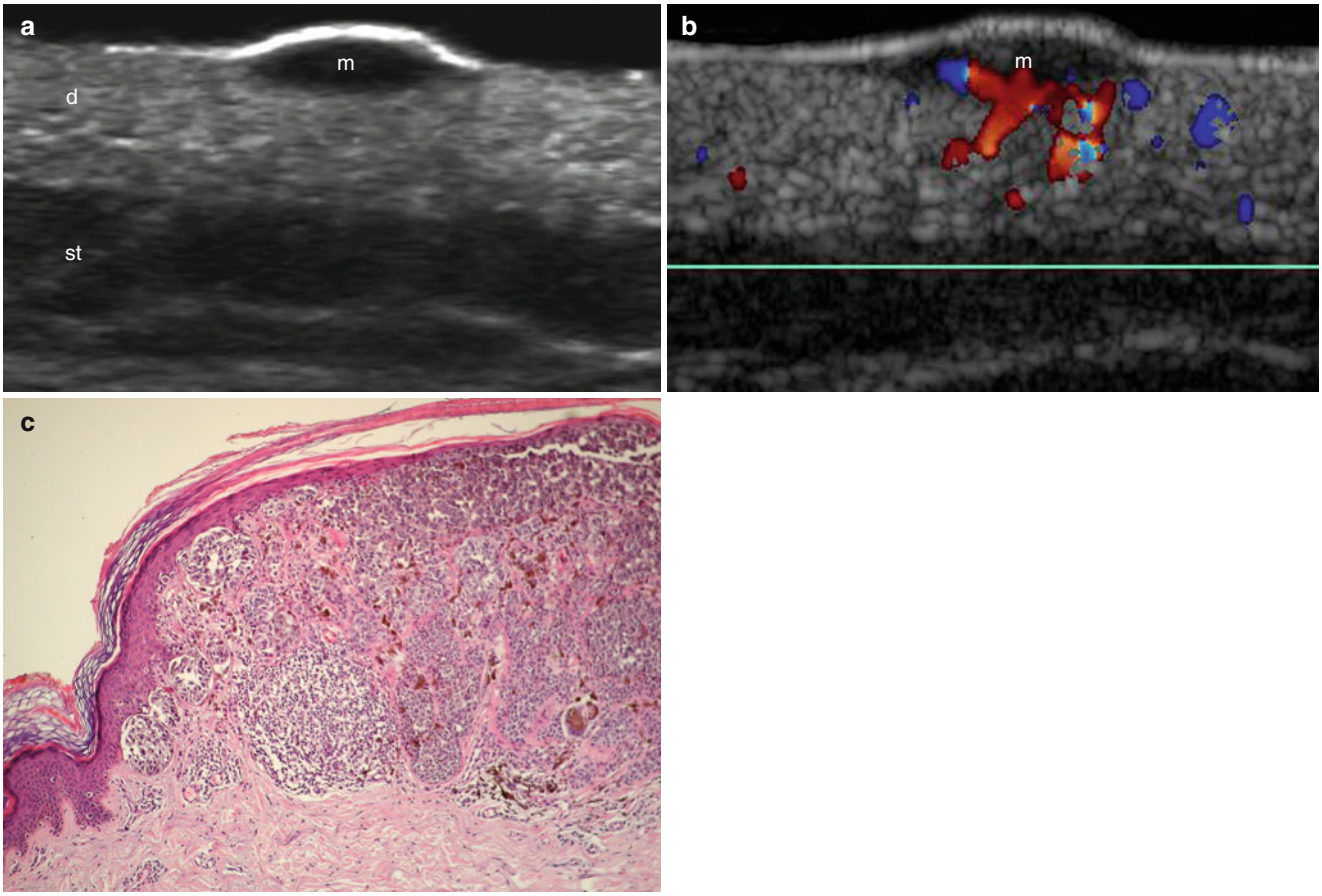

Fig. 9.14 (**a**–**c**) Melanoma. (**a**) Grey scale ultrasound image (transverse view) in the dorsal region shows a well-defined fusiform-shaped hypoechoic lesion (*m*) in the dermis. (**b**) Color Doppler ultrasound image (transverse view) demonstrates increased vascularity within the tumor (m). (**c**) Histology (HE 40 × zoom): melanocytic proliferation composed by nests of different sizes in the dermo-epidermal junction and the dermis. Fibrous stroma and melanophages surround the atypical cells. *Abbreviations*: *d* dermis, *st* subcutaneous tissue, *m* melanoma

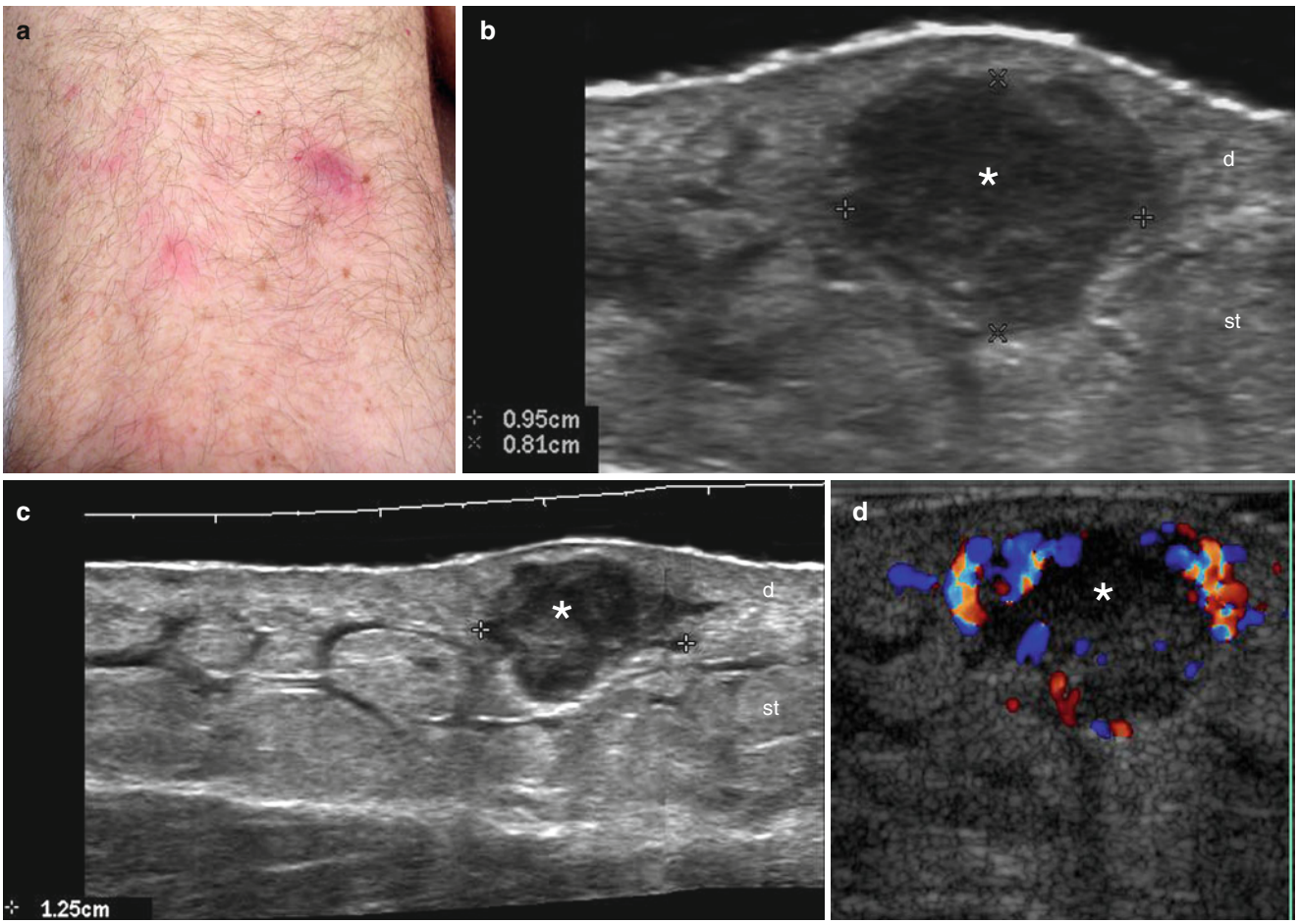

Fig. 9.15 (**a**–**d**) Melanoma in-transit metastasis. (**a**) Clinical image shows erythematous papules in the dorsum of the left thigh. The patient has history of a melanoma surgery in the left ankle. (**b**, **c**) Grey scale images (**b** zoomed, transverse view and **c** extended field of longitudinal view of the large size cutaneous lesion) demonstrate 1.25 × 0.81 cm oval-shaped hypoechoic structure located in the dermis and subcutaneous tissue. Increased echogenicity and septal anechoic bands in the surrounding subcutaneous tissue suggestive of edema are also detected. (**d**) Color Doppler ultrasound image (transverse view) shows increased blood flow in the periphery of the lesion

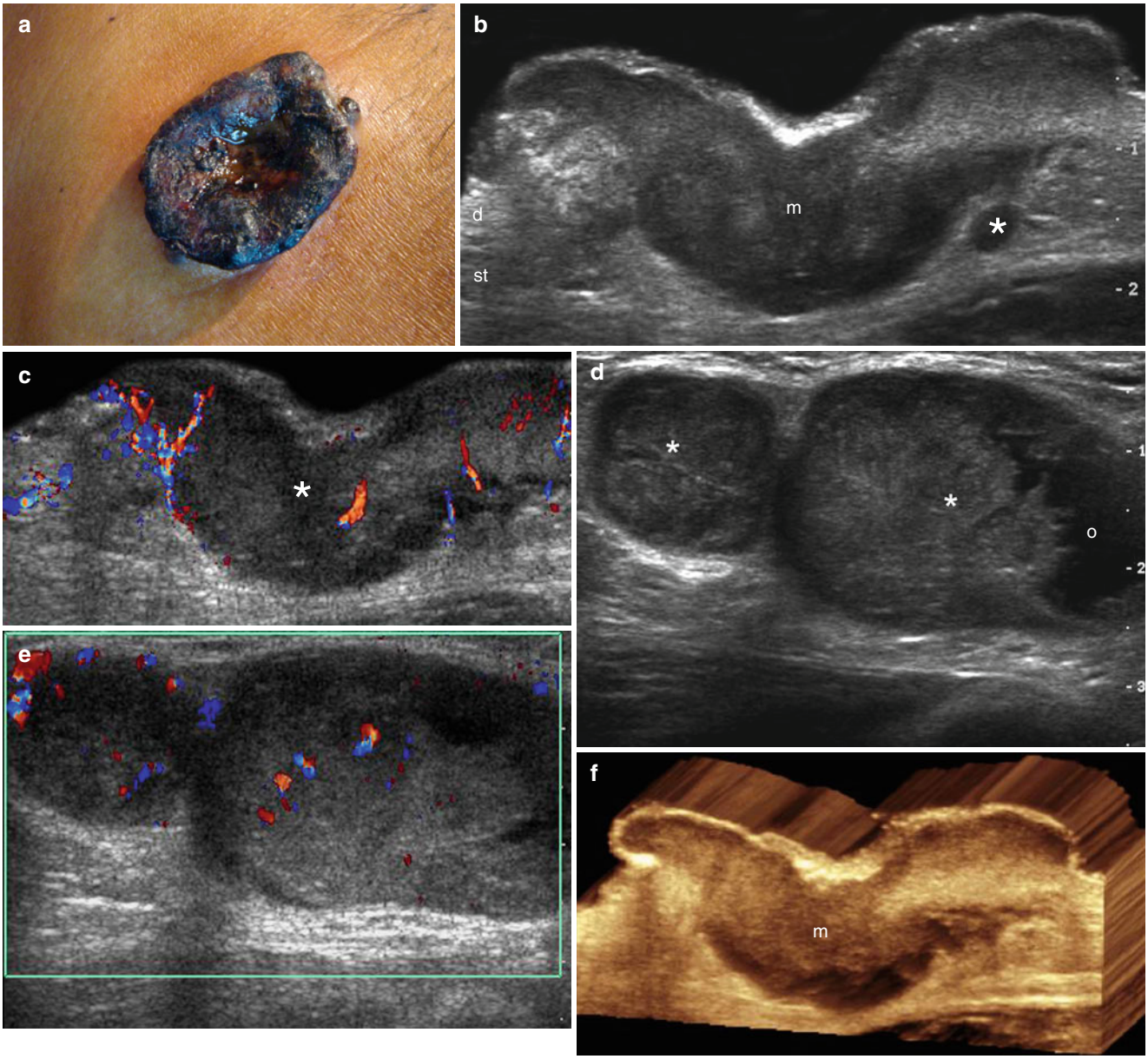

Fig. 9.16 (**a**–**f**) Primary melanoma, satellite and nodal metastasis. (**a**) Clinical photograph shows exophytic and ulcerated hyperpigmented lesion in the right aspect of the abdominal wall. (**b**) Grey scale ultrasound image (transverse view) demonstrates a well-defined fusiform-shaped hypoechoic solid structure (*m*) that involves the epidermis, dermis, and subcutaneous tissue. Notice the satellite nodule (*) located in the subcutaneous tissue adjacent to the main lesion. (**c**) Color Doppler ultrasound image (transverse view) shows increased vascularity in the lesional area. (**d**) Grey scale ultrasound image (transverse view, right axilla) demonstrates two well-defined, oval-shaped structures located in the subcutaneous tissue suggestive of nodal metastases. Notice the anechoic area (*o*) in one of the lesions. (**e**) Color Doppler ultrasound image (transverse view) shows increased blood flow with an asymmetric and irregular pattern within the nodules. (**f**) 3D reconstruction of the lesion (transverse view, 5–8 s sweep)

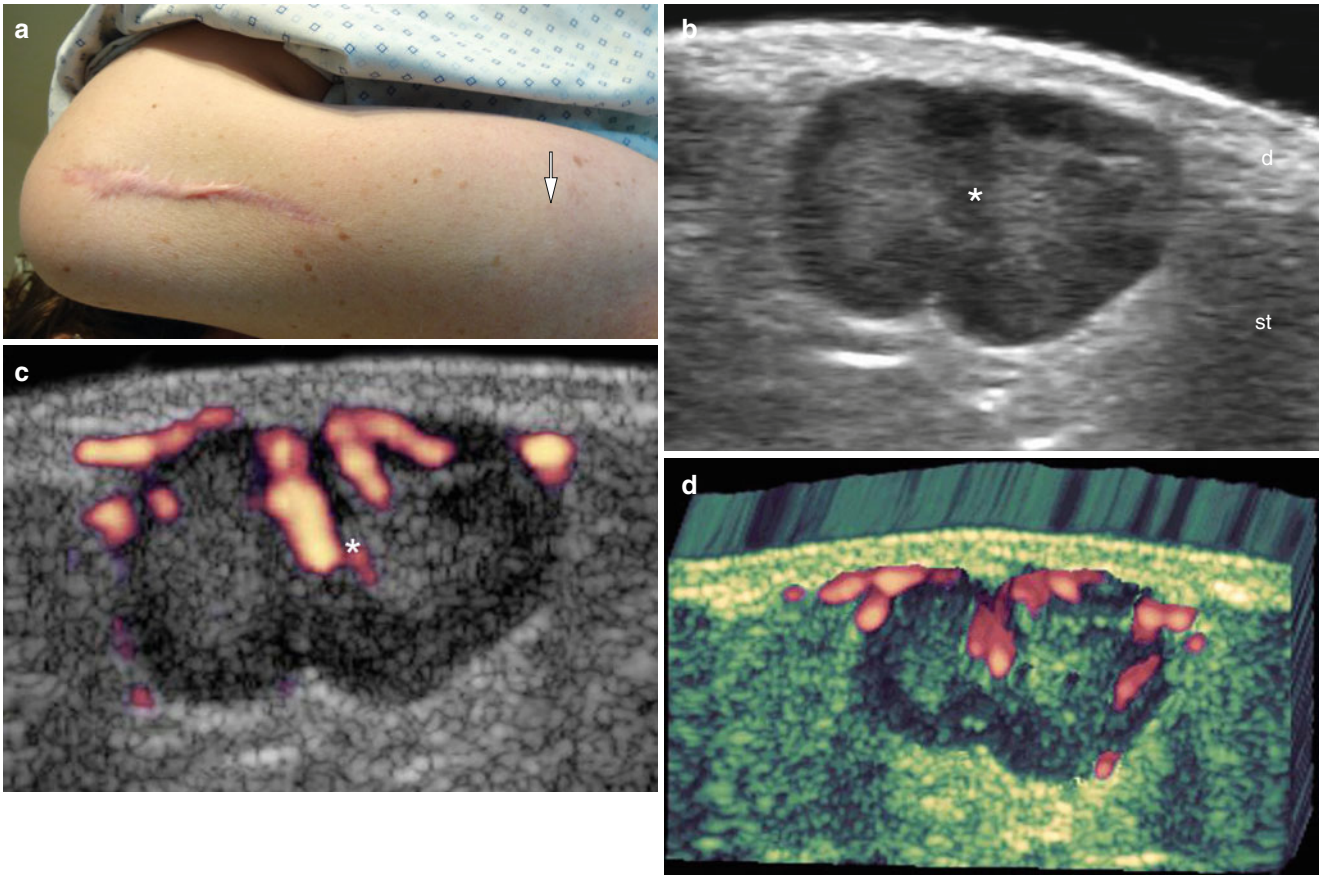

Fig. 9.17 (**a**–**d**) Melanoma in-transit metastasis. (**a**) Clinical photograph shows a patient with a history of a recent melanoma surgery in the left arm and a palpable lump (*arrow*) distal to the scar. (**b**) Grey scale (transverse view) demonstrates a well-defined, oval-shaped lobulated solid structure (*) in the subcutaneous tissue that bulges into the dermis. The nodule presents a hypoechoic rim and a slightly hyperechoic center. (**c**) Power Doppler image (transverse view) shows increased vascularity within the nodule (*) with thick and irregular vessels. (**d**) 3D power angio Doppler reconstruction of the lesion (5–8 s sweep)

9.3.1 Contrast-Enhanced Ultrasound in Melanoma

Intravenous contrast medium, conformed by gas-filled microbubbles that enhance the echogenicity of the vessels, has been progressively used in melanoma and loco-regional staging for obtaining early information about the effectiveness of the treatment of the primary lesion and clarifying a doubtful cortical thickening at the lymph nodes [27–29]. It is also a promising tool to reduce the number of patients who should undergo fine-needle aspiration cytology of lymph nodes with focal cortical thickening in melanoma [33, 34]. The vascular density in melanoma has already been correlated with metastatic potential using color Doppler ultrasound. Thus, neovascularization has been reported as a prognostic factor for metastasis equivalent to the Breslow index [35]. Furthermore, contrast-enhanced ultrasound imaging of tumor neovascularity has been mentioned in the literature as providing a noninvasive marker of angiogenesis corresponding to the expression of vascular endothelial growth factor in mice that were implanted with the human melanoma cell line DB-1 that can become a useful tool for monitoring clinical anti-angiogenic therapies [36]. Lymphosonography (i.e., contrast-enhanced ultrasound after interstitial injection of a contrast agent) has been reported as statistically better than lymphoscintigraphy for the detection of sentinel lymph nodes in an animal model [37].

The limitations of the usage of contrast medium are the current short-life time of the bubbles within the systemic circulation that commonly provides minutes for performing the analysis, the cost, and the invasive nature of the intravenous injection. Nevertheless, lymphosonography can require seconds to identify the movement of the contrast within lymphatic channels and present a higher spatial resolution than lymphoscintigraphy. The sonographic signs for malignancy in lymphosonography are heterogenous or sparse enhancement in sentinel lymph nodes. In contrast, uniform enhancement in small (<5 cm) sentinel lymph nodes suggest benignancy [37]. Thus, contrast-enhanced ultrasound can improve the management of melanoma by allowing detection and characterization of the primary and secondary lesions, guidance of biopsy, and prompt assessment of the effectiveness of the pharmacodynamic response [31].

9.3.2 Elastography in Cutaneous Melanoma

As of yet, few reports that show the experience or usefulness of sonoelastography in cutaneous melanoma are available [38, 39]. There are reports on acousto-optical elastography, an experimental imaging modality for quantifying the mechanical behavior of skin lesions. The method relies on stimulating the tissue with a low frequency acoustic force and imaging the resulting strains in the tissue by means of quantifying the magnitude of the dynamic shift in a back-reflected laser speckle pattern from the skin. The magnitude of the shift reflects the local stiffness of the tissue, which has shown promising results when comparing benign melanocytic nevi with melanoma [40]. However, to date there are no reports that have altered management in terms of detecting undisclosed malignancies, although it may increase the diagnostic confidence of less-experienced operators performing ultrasound. Therefore, the assessment of the role of elastography in melanoma and other cutaneous tumors probably will require further investigation [37].

9.3.3 High-Intensity Focused Ultrasound in Cutaneous Melanoma

High-intensity focused ultrasound (HIFU) is a focused sonic energy that heats and destroys the tissue through thermal ablation. Currently, scarce reports on the effects of HIFU in melanoma are available. However, significant tumor necrosis and absent local serum-vascular endothelial growth factor have been described in animal models [41, 42].

Tips for Melanoma

- Hypoechoic
- Fusiform lesion
- Increased vascularity
- Check for satellite (≤2 cm from the primary tumor), in-transit (≥2 cm from the primary tumor), or nodal metastasis
- Provide extension in all axes

9.4 Other Malignant Skin Tumors

9.4.1 Dermatofibrosarcoma Protuberans

Dermatofibrosarcoma protuberans (DFSP) is an unusual, locally aggressive cutaneous fibroblastic neoplasm that mainly affects the torso and proximal extremities of young and middle-aged adults. DFSP presents as a slow-growing, multinodular, and plaque-like erythematous or purple mass that tends to infiltrate and show local recurrence but rarely metastasizes to distant organs [43].

On histology, there is a proliferation of spindle cells with elongated nuclei with little or no pleomorphism. DFSP usually affects the dermis and subcutaneous tissue although it can also involve deeper layers. Inmunohistochemical markers such as CD34 are commonly positive [43, 44]. On sonography, two sonographic patterns have been described The first is a well-defined oval hypoechoic structure and the second is composed of an ill-defined heterogeneous structure, with hyper- and hypoechoic areas and lobulated or pseudopodia-like protrusions commonly affecting the dermis and subcutaneous tissue. DFSP can also send projections to the fascial or muscular layers. Nevertheless, this condition usually tends to spread horizontally, and the degree of vascularization is variable but commonly presents slow flow vessels [45, 46] (Figs. 9.18 and 9.19).

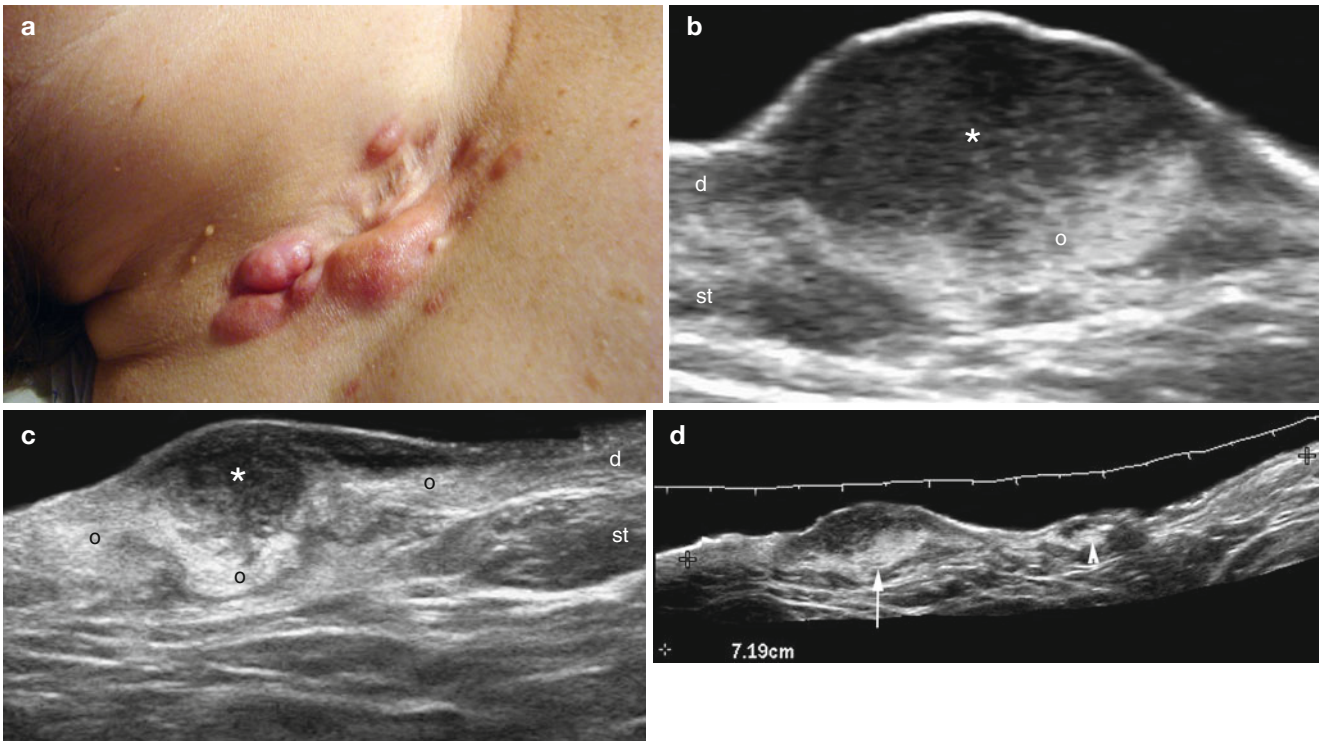

Fig. 9.18 (**a**–**h**) Dermatofibrosarcoma protuberans. (**a**) Clinical image shows erythematous lumps in the right aspect of the neck. (**b**–**d**) Grey scale ultrasound images (**d**: zoomed longitudinal view; **c** transverse view; **d** extended field of longitudinal view) demonstrate a 7.19 cm long, ill-defined mixed echogenicity lesion that involves the dermis and subcutaneous tissue. The lesion is composed of a superficial lobulated hypoechoic pseudonodular region (*) and a deep hyperechoic region (o). Notice the two pseudonodular regions in figure (**d**) that present a large size (*arrow*) and small size (*arrowhead*) lesion. (**e**) Color Doppler ultrasound image (transverse view) demonstrates increased vascularity within the lesion. (**f**) 3D power angio reconstruction of the tumor (5–8 s sweep). (**g**) The tumor at surgery. (**h**) Histology (HE 100× zoom): atypical spindle cell proliferation that surrounds adipocytes

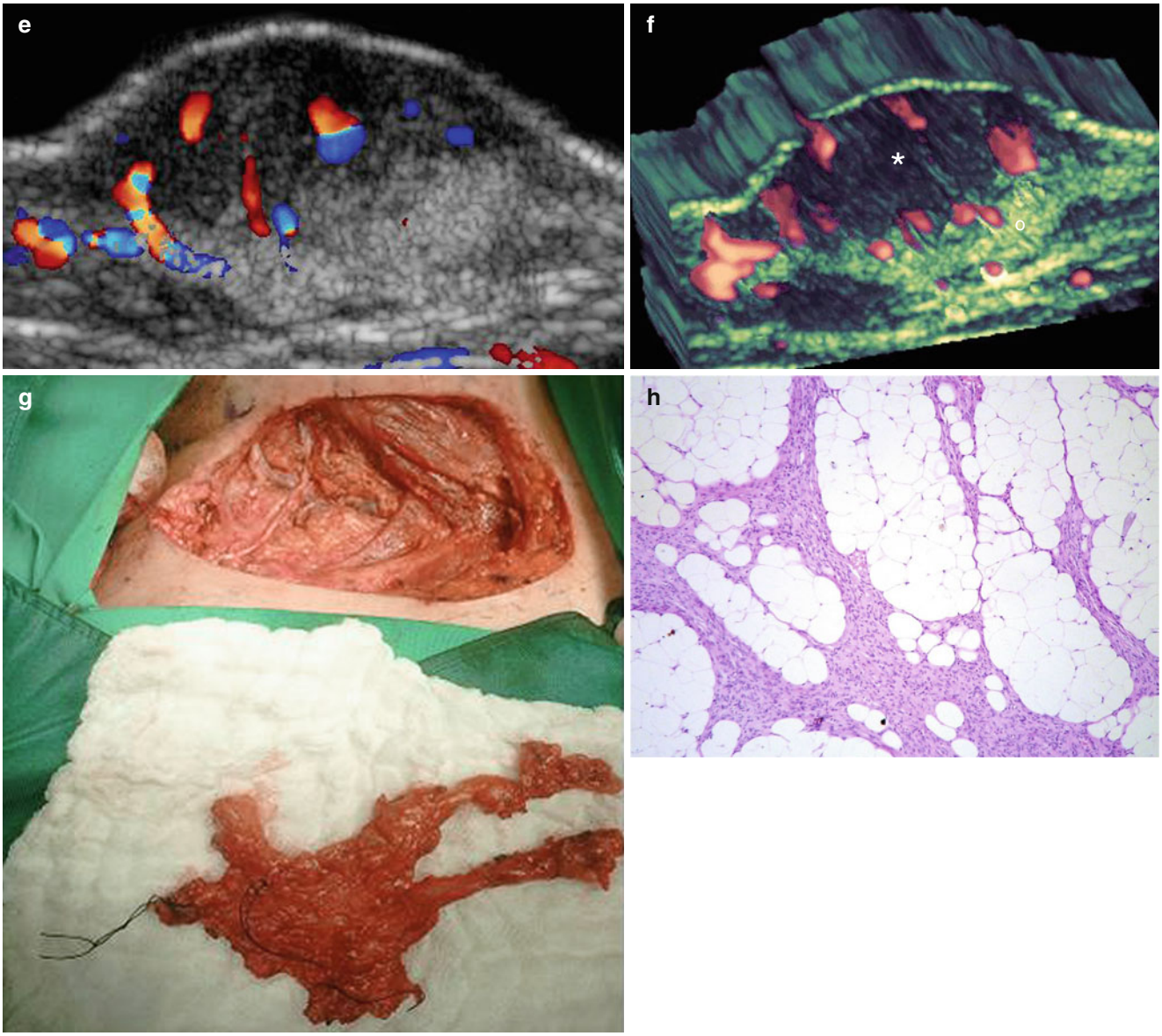

Fig. 9.18 (continued)

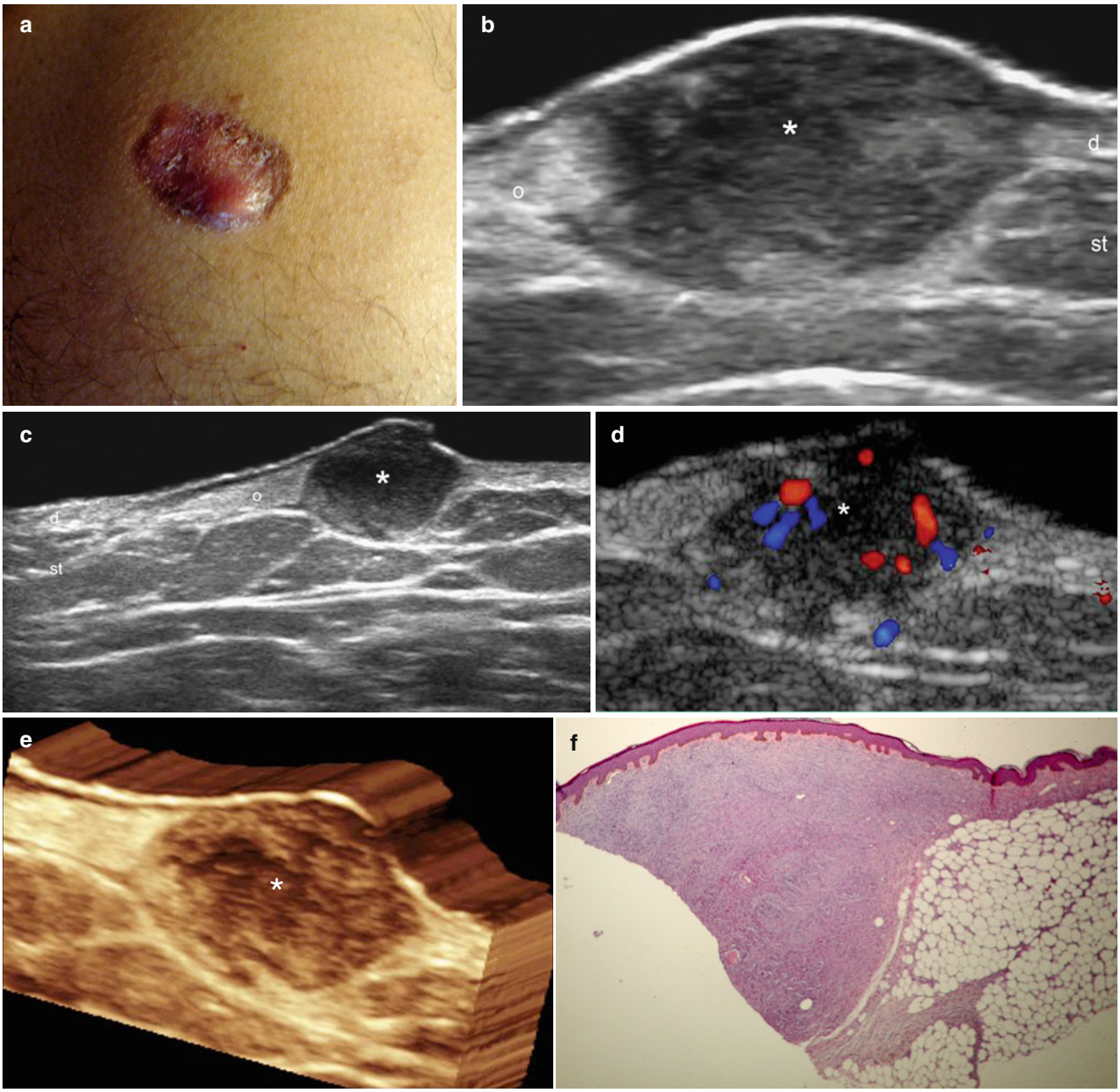

Fig. 9.19 (**a**–**f**) Dermatofibrosarcoma protuberans. (**a**) Clinical photograph shows an erythematous lump in the right thigh. (**b**, **c**) Grey scale ultrasound images (**b** transverse view; **c** longitudinal view) demonstrate ill-defined mixed echogenicity lesion located in the dermis and subcutaneous tissue. It presents a superficial hypoechoic and lobulated pseudonodular part (*) and an increased echogenicity (o) of the vicinity. (**d**) Color Doppler ultrasound image (longitudinal view) shows increased blood flow within the hypoechoic part. (**e**) 3D reconstruction of the lesion (*, 5–8 s sweep, transverse view). (**f**) Histology (HE 20 × zoom): dermal and hypodermal proliferation of atypical spindle cells. *Abbreviations*: *d* dermis, *st* subcutaneous tissue

9.4.2 Cutaneous Angiosarcoma

Cutaneous angiosarcoma is a rare malignant tumor of endothelial origin that often presents an aggressive course, with 60 % of angiosarcomas primarily located in the skin and mainly affect older patients (>50 years of age) with a peak incidence in the eighth decade. The 5-year survival rate ranges from 12 % to 20 % and angiosarcoma often undergoes distant metastasis most commonly in the liver, lymph nodes, and spleen. The most important prognostic feature is tumor size, and other significant factors are depth of invasion >3 mm, mitotic rate, positive surgical margins, local recurrence, and metastases.

The head and neck form of angiosarcoma is the most frequent subtype, also called idiopathic angiosarcoma, and accounts for 50–60 % of all cases. The latter form is frequently seen on the scalp of elderly men.

Clinically, angiosarcomas show as a bruise-like erythematous or violaceous plaques or mass that becomes larger and ill-defined over time. Pain, bleeding, and swelling have been also described. A higher incidence of angiosarcomas occurs in female patients that have received radiation therapy for breast cancer, patients that present with chronic extremity lymphedema (Stewart-Treves syndrome), and pre-existing vascular malformations have been reported [47, 48].

Histologically, the masses consist of ill-defined hemorrhagic and occasionally blood-filled cystic spaces. The cutaneous layers and sometimes deeper structures are commonly replaced by a diffuse, irregular, and anastomosing network of endothelial-lined erythrocyte containing variably slit-like to medium-sized sinusoidal to larger blood-filled cystic spaces. The endothelial cells are enlarged and contain hobnailed hyperchromatic round to oval nuclei with condensed chromatin. Other forms show a solid pattern with epithelioid and spindle cells with little intervening stroma [49–51].

On sonography, angiosarcoma appears as an ill-defined or lobulated hypoechoic mass with prominent vascularity commonly with low flow arterial and venous vessels. This tumor usually infiltrates the dermis and subcutaneous tissue but can also affect deeper structures. (See Fig. 8.10.)

9.4.3 Kaposi's Sarcoma

Kaposi's sarcoma (KS) is a low-grade mesenchymal tumor involving blood and lymphatic vessels. There are four variants of the disease, each presenting a different clinical manifestation: classic or sporadic, African or endemic, organ transplant-related or iatrogenic, and AIDS-related or epidemic. This condition is the most common tumor among patients with HIV infection [52]. KS is a low-grade malignancy that is associated with human herpesvirus-8, and composes a multifocal tumor that most commonly affects mucocutaneous sites. It might also involve lymph nodes and visceral organs, in particular of the respiratory and gastrointestinal tract, but it can affect every organ system [53].

Histologically, in its early stages, KS contains blood vessels with a fine endothelium passing through the dermal collagen bundles. In the plaque and nodular stages, the vessel lumens are visible more clearly and there is a progressive increase in the number of neoplastic spindle cells with a low degree of pleomorphism and atypia, and occasional mitoses. The infiltrate is made up of lymphocytes and plasma cells [54].

On sonography, KS lesions appear as hypoechoic or heterogeneous lesions, as a plaque-like thickening of the dermis, sometimes with a nodular appearance. Vascularity is variable within the lesion and infiltration of deeper structures, such as muscles, has been reported [55]. Ultrasound has been used as an objective tool for measuring the degree of remission of the disease [56, 57] (See Fig. 8.11).

9.4.4 Merkel Cell Carcinoma

Merkel cell carcinoma (MCC) originates from a cutaneous mechanoreceptor cell (Merkel cell) located in the basal layer of the epidermis [58]. MCC is a rare neuroendocrine carcinoma of the skin that is found primarily in older individuals and exhibits a bad prognosis mainly because of a high rate of local recurrence. Risk factors associated with the development of MCC include exposure to ultraviolet radiation and immunosuppression, with a viral etiology (polyomavirus) also being proposed. Thirty-six percent of cases of MCC are located on sun-exposed areas such as the face and 50 % are located on the head and neck.

MCC presents clinically as a single firm flesh-colored to erythematous dome-shaped nodule with a smooth shiny surface, sometimes with telangiectasia.

Regional lymph nodes are involved in 15–66 % of patients and distant metastases are found in 1–6 % of patients.

Histologically, MCC appears as a dermal nodule or plaque that frequently extends into the subcutaneous tissue. It may show a nodular or infitrative pattern with lymphovascular invasion. Small blue cells with basophilic nuclei and minimal cytoplasm are detected. Mitoses are frequent and apoptosis index is high. Inmunohistochemistry using CK (cytokeratin)-20 positive and thyroid transcription factor-1 negative may help to assess the diagnosis, among other markers.

Tumor size ≥2 cm, lymph node involvement, deeper structure involvement (muscle, fascia or cartilage), infiltrative pattern on histology, and distant metastasis (liver, lung, bone, brain) present a worse prognosis [59].

On sonography, MCC tumors will present as a hypoechoic ill-defined nodule or mass that usually affects the dermis and subcutaneous tissue and presents prominent vascularity (Fig. 9.20).

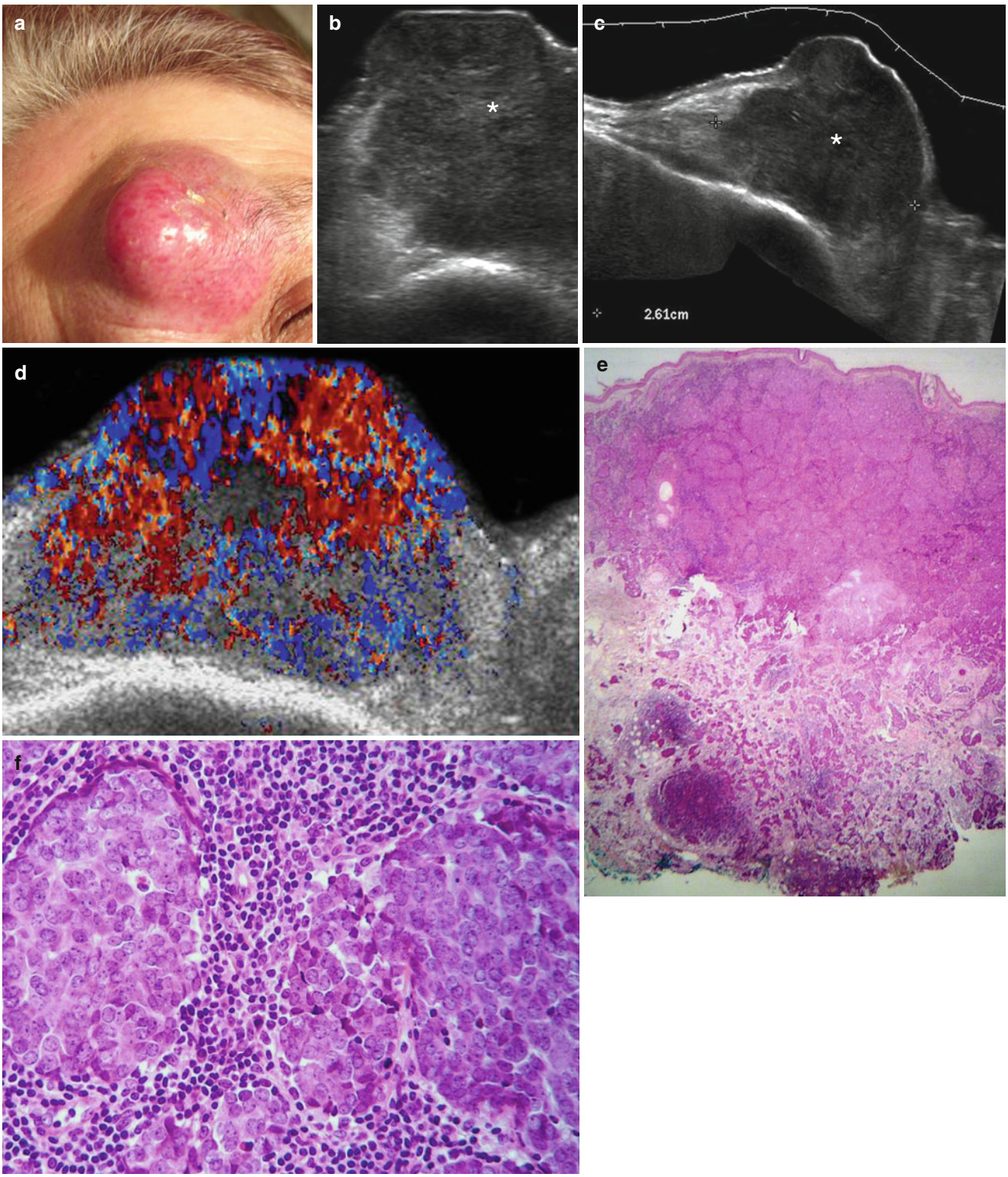

Fig. 9.20 (**a**–**f**) Merkel cell carcinoma. (**a**) Clinical photograph shows erythematous and exophytic lump in the medial aspect of the left frontal region. (**b**, **c**) Grey scale ultrasound images (**b** zoomed transverse view; **c** longitudinal view) demonstrate a 2.61 cm long oval-shaped hypoechoic solid mass with irregular borders that involves the dermis and subcutaneous tissue. (**d**) Color Doppler ultrasound image (transverse view) shows prominent vascularity within the mass. (**e**, **f**) Histology (e: HE × 20 zoom; f: HE× 400 zoom) demonstrates dense and irregular aggregates of pyknotic cells with little cytoplasm, fine chromatin, and lymphoid stroma. Immunohistochemically, the neoplastic cells stained positive for chromogranin, synaptophysin, and perinuclear cytokeratin 20

9.4.5 Cutaneous Lymphoma

Cutaneous lymphoma comprises a heterogeneous group of lymphoproliferative cutaneous disorders separated mainly by the predominant type of lymphoid cell present in the tumor. Hence, they can be classified into two groups: T-cell and B-cell lymphomas [60]. The most common type of T-cell lymphomas are mycosis fungoides, named for its mushroom-like tumors that are commonly seen at the end stage of the disease and Sezary's syndrome, a leukemic erythrodermic lymphoma variant. The three major histological subgroups of primary cutaneous B-cell lymphoma are: follicle center, marginal zone B-cell, large B-cell and leg type.

9.4.5.1 Mycosis Fungoides

Mycosis fungoides is the most frequent form of primary cutaneous T-cell lymphoma that is a low-grade cutaneous lymphoma characterized by skin-homing CD4+ T cells. Clinically, it shows highly symptomatic progressive skin lesions including patches, plaques, tumors, scaling, poikiloderma, and erythroderma, and has a poorer prognosis during later stages [61].

Histologically, mycosis fungoides presents as hyperkeratosis, psoriasiform hyperplasia, and superficial perivascular lymphocytic infiltrates. Scarring and atypical lymphocytes with hyperchromatic nuclei can also present. Folliculotropic mycosis fungoides (FMF) is a variant of cutaneous T-cell lymphoma that affects the hair follicles.

9.4.5.2 Sezary's Syndrome

The leukemic form of Sezary's syndrome is most common in the fifth to seventh decades of life and is characterized by intense pruritus, edema, scaling (especially in the palms and soles [palmoplantar keratoderma]), and a generalized infiltrative erythroderma. Lymphadenopathy and atypical circulating lymphocytes (Sezary's cells) in the peripheral blood are also commonly found.

Histologically, Sezary's syndrome shows infiltrates composed of highly convoluted cerbriform lymphocytes with hyperkeratosis, acanthosis, and sometimes microabscesses.

9.4.5.3 Subcutaneous Panniculitic T-Cell Lymphoma

Subcutaneous panniculitic T-cell lymphoma is a less common form of presentation of T-cell lymphoma that can clinically mimic chronic panniculitis and present as multiple ulcerated and erythematous or violaceous nodules or plaques that most commonly affect the torso and extremities. Histologically, panniculitic T-cell lymphoma presents with vesicular and hyperchromatic nuclei and conspicuous erythrophagocytosis. The atypical lymphocytes involve the subcutaneous tissue and rim fat cells with a lace-like appearance. Fat necrosis with xanthoma cells and hemorrhage are also commonly found.

9.4.5.4 B-Cell Cutaneous Lymphomas

B-cell cutaneous lymphomas cab be either primary or metastatic. The marginal zone B-cell lymphoma is the most common primary cutaneous type. Clinically, this type shows as single or multiple asymptomatic, erythematous, brown or violaceous papules, nodules, or plaques sometimes surrounded by an erythematous border. The torso, especially the back, is the most affected area. In contrast to mucosae, the skin does not have an associated B-cell lymphocyte population, therefore it has been suggested that skin-associated lymphoid tissue may develop following chronic antigen stimulation, such as chronic inflammation or autoimmune diseases. Histologically, there is a dense atypical B-cell lymphoid infiltrate in B-cell cutaneous lymphoma that dissects the collagen with inmunoblasts that present central eosinophilic nuclei and scattered eosinophils [62].

On sonography, lymphomas can present as focal hypoechoic or heterogeneous thickening of the dermis or as diffuse lesions that involve the dermis and subcutaneous tissue. The diffuse form of presentation usually appears as heterogeneous involvement with mixed echogenicity (anechoic, hypoechoic, and hyperechoic areas). When the lesions are anechoic, they can mimic fluid collections. Diffuse forms of presentation may show single or multiple locations and anechoic or hypoechoic plaque-like structures. Subcutaneous panniculitic T-cell lymphoma (STCL) can present with prominent and hyperechoic fatty lobules as well as anechoic or hypoechoic septa in the subcutaneous tissue. The latter form of presentation (STCL) may mimic cellulitis. The vascularity is variable and can go from hypovascular to hypervascular (63, 64) (Figs. 9.21, 9.22, 9.23, and 9.24).

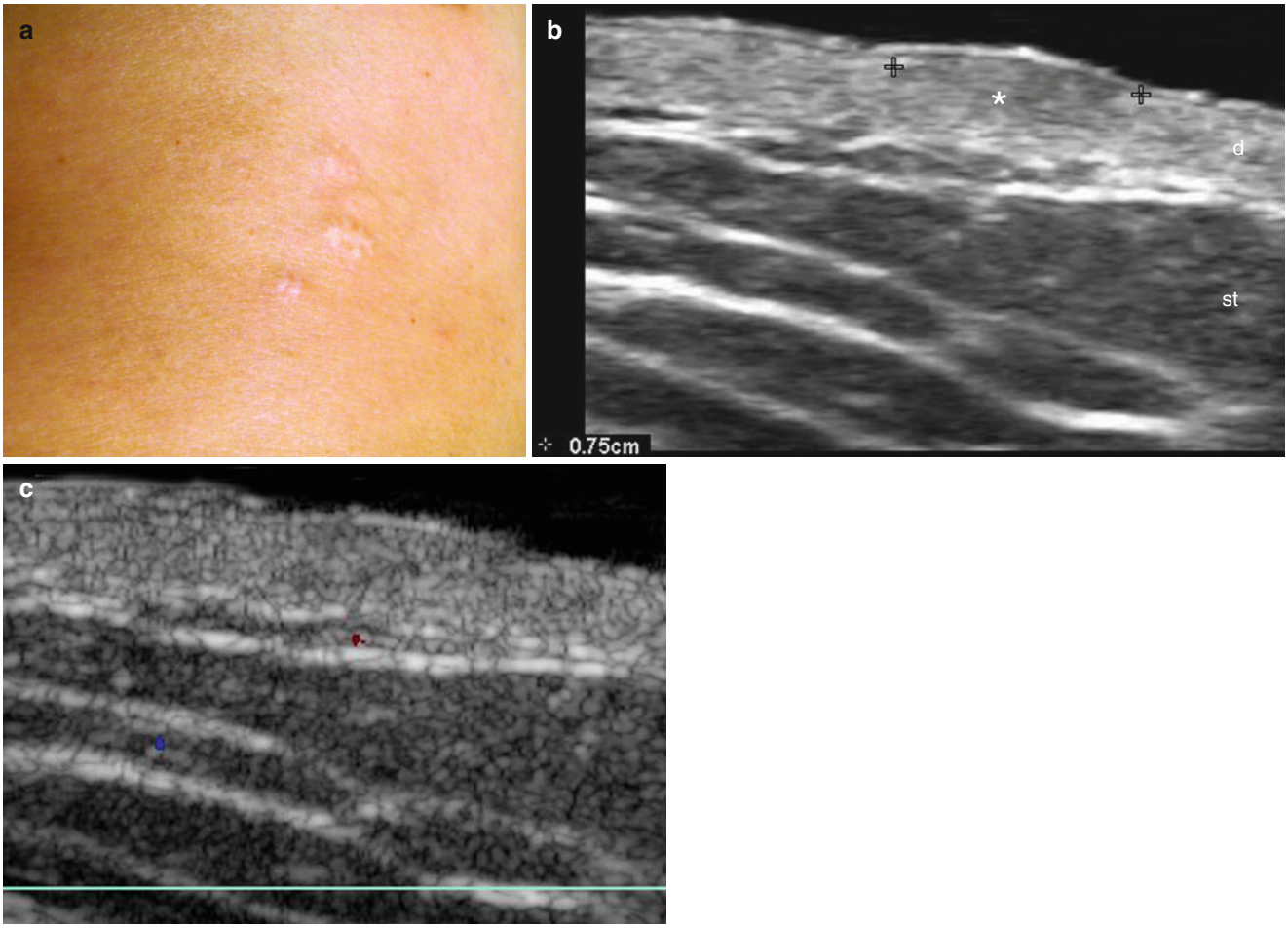

Fig. 9.21 (**a**–**c**) Cutaneous lymphoma (mycosis fungoides). (**a**) Clinical image shows hypopigmented lumps in the left side of the anterior aspect of the thoracic region. (**b**) Grey scale ultrasound image (longitudinal view) demonstrates 0.75 cm ill-defined hypoechoic and heterogeneous structure (*) in the dermis. (**c**) Color Doppler ultrasound image (longitudinal view) demonstrates no signs of hypervascularity in the lesional region

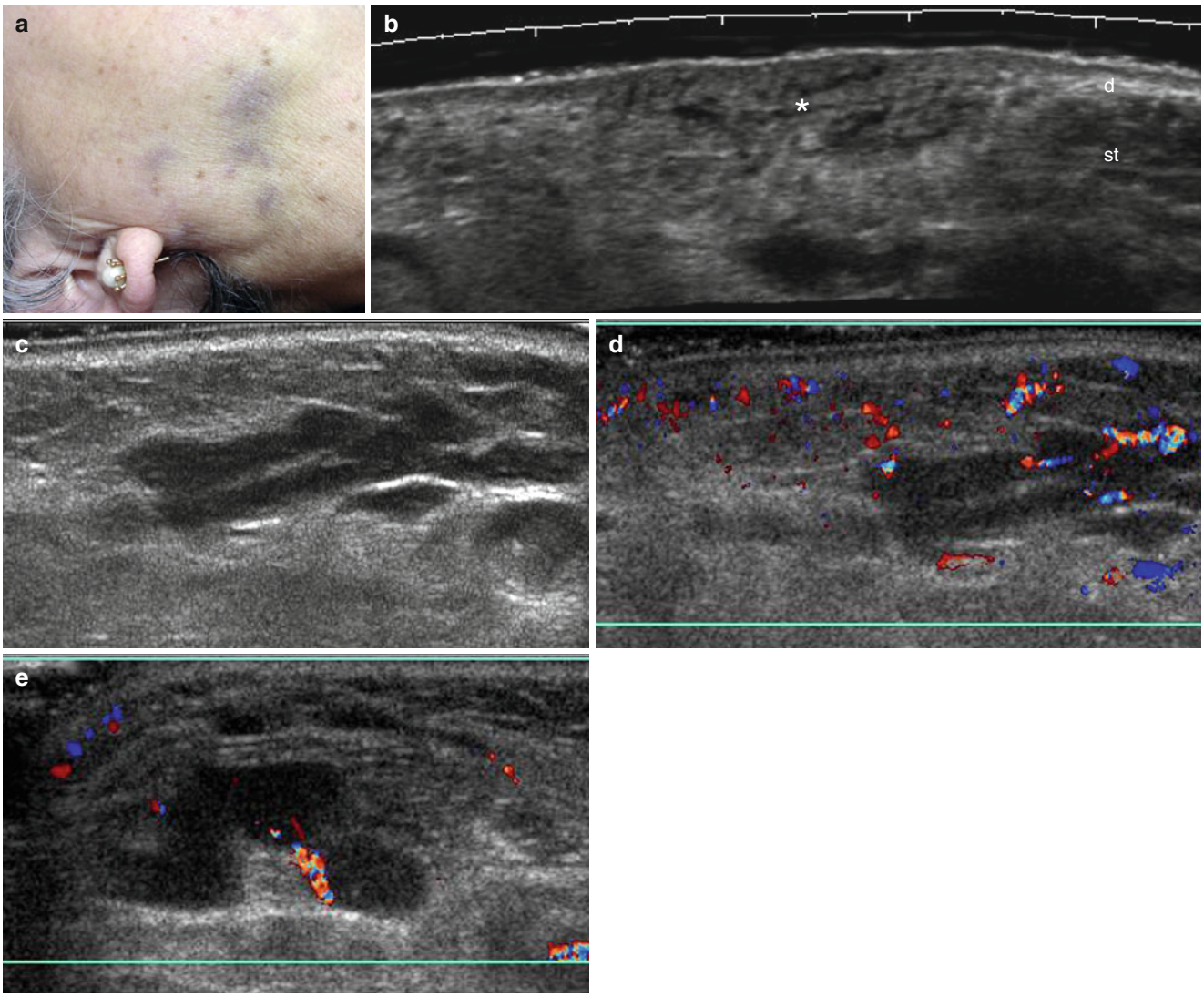

Fig. 9.22 (**a**–**e**) Cutaneous lymphoma. (**a**) Clinical photograph shows purple bruise-like lesions in the right mandible and neck regions. (**b**) Grey scale ultrasound image (transverse view) demonstrates ill-defined heterogeneous echogenicity area (*) in the dermis and subcutaneous tissue. (**c**) Grey scale ultrasound image (longitudinal view) presents hypoechoic plaque-like structures in the subcutaneous tissue. (**d**) Color Doppler ultrasound image (longitudinal view) shows increased vascularity in the lesional region. (**e**) Color Doppler ultrasound image (transverse view, neck region) demonstrates oval-shaped hypoechoic nodules with loss of the hyperechoic center and compatible with infiltrated lymphadenopathies

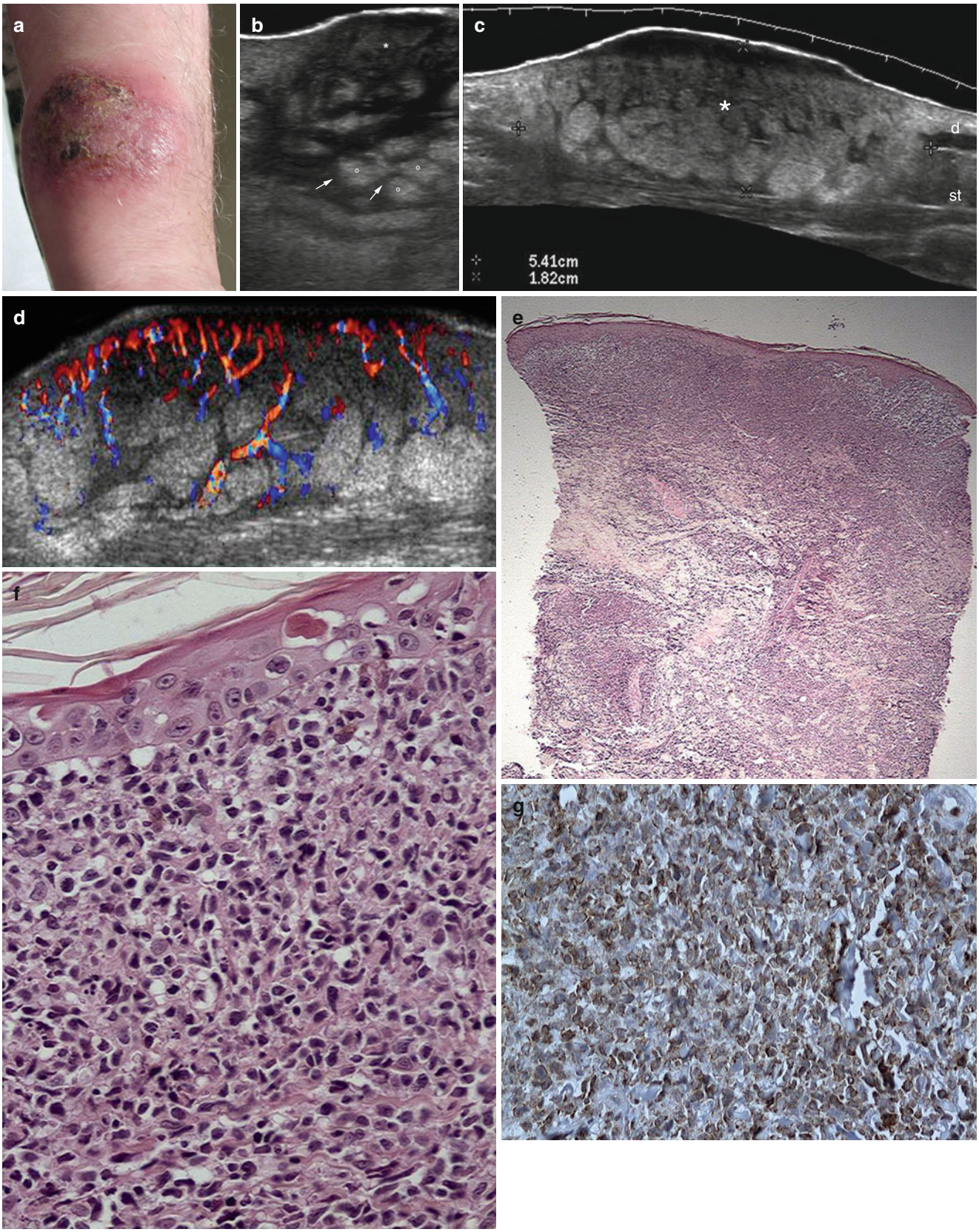

Fig. 9.23 (**a**–**g**) Subcutaneous panniculitic T-cell lymphoma. (**a**) Clinical photograph shows a crusty and erythematous lesion in the left arm. (**b**, **c**) Grey scale ultrasound images (**b** zoomed and **c** extended field of longitudinal views) demonstrats a 5.41 × 1.82 cm focal area (*, between markers) that presents increased thickness of the dermis and subcutaneous tissue with hypoechogenicity of the dermis and hyperechogenicity of the subcutaneous tissue. Notice the prominent and hyperechoic fatty lobules (o) and the thick and hypoechoic septa (*arrows*) in the subcutaneous tissue with a "cobblestone" appearance. (**d**) Color Doppler ultrasound image (longitudinal view) shows increased vascularity in the lesional region. (**e**, **f**) Histology (e: HE ×20 zoom; f: HE ×40 zoom) demonstrates a dense infiltrate with atypical lymphoid cells. (**g**) Immunohistochemistry (400× zoom) shows CD 3 positive T-lymphoid cells

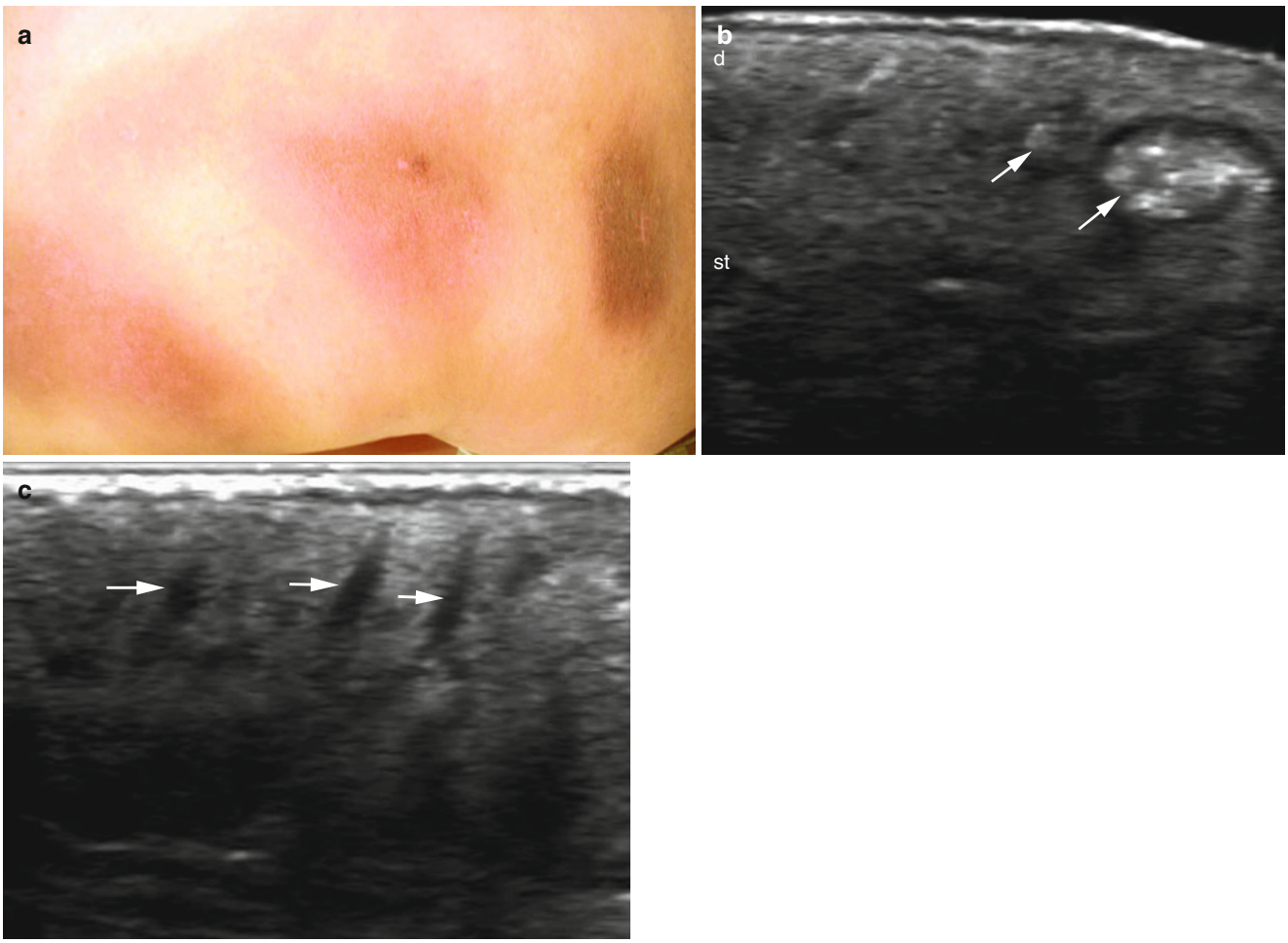

Fig. 9.24 (**a**–**c**) Folliculotropic mycosis fungoides (FMF). (**a**) Clinical photograph shows erythematous and slightly pigmented indurations in the dorsal region. (**b**, **c**) Grey scale ultrasound images (transverse views) demonstrate round and oval-shaped, hyperechoic deposits (*arrows*) attached to the dermal hair follicles (Figure b). Notice that the hair follicles are also enlarged (*arrows* in figure c)

References

1. Hong H, Sun J, Cai W. Anatomical and molecular imaging of skin cancer. Clin Cosmet Investig Dermatol. 2008;1:1–17.
2. Bartoš V, Pokorný D, Zacharová O, Haluska P, Doboszová J, Kullová M, et al. Recurrent basal cell carcinoma: a clinicopathological study and evaluation of histomorphological findings in primary and recurrent lesions. Acta Dermatovenerol Alp Panonica Adriat. 2011;20:67–75.
3. Goto M, Kai Y, Arakawa S, Oishi M, Ishikawa K, Anzai S, et al. Analysis of 256 cases of basal cell carcinoma after either one-step or two-step surgery in a Japanese institution. J Dermatol. 2012;39:68–71.
4. Brenn T, Mc Kee P. Tumors of the surface epithelium. In: Mc Kee P, Calonje E, Granter S, editors. Pathology of the skin with clinical correlations. 3rd ed. Philadelphia: Elsevier/Mosby; 2005. p. 1167–82.
5. Samarasinghe V, Madan V, Lear JT. Management of high-risk squamous cell carcinoma of the skin. Expert Rev Anticancer Ther. 2011;11:763–9.
6. Veness MJ. High-risk cutaneous squamous cell carcinoma of the head and neck. J Biomed Biotechnol. 2007;2007(3):80572.
7. Brenn T, Mc Kee P. Tumors of the surface epithelium. In: Mc Kee P, Calonje E, Granter S, editors. Pathology of the skin with clinical correlations. 3rd ed. Philadelphia: Elsevier/Mosby; 2005. p. 1199–228.
8. Gniadecki R, Normal DT. Basal cell carcinoma—clinical guidelines, Danish dermatological society. Forum for Nord Derm Ven. 2009;14(1):4–6.
9. Zavos G, Karidis NP, Tsourouflis G, Bokos J, Diles K, Sotirchos G, et al. Nonmelanoma skin cancer after renal transplantation: a single-center experience in 1736 transplantations. Int J Dermatol. 2011;50:1496–500.
10. Yuen WY, Jonkman MF. Risk of squamous cell carcinoma in junctional epidermolysis bullosa, non-Herlitz type: report of 7 cases and a review of the literature. J Am Acad Dermatol. 2011;65:780–9.
11. Huang L, Wong YP, Burd A. A novel homozygous splice site mutation in COL7A1 in a Chinese patient with severe recessive dystrophic epidermolysis bullosa and squamous cell carcinoma. Int J Dermatol. 2011;50:52–6.
12. Bobadilla F, Wortsman X, Muñoz C, Segovia L, Espinoza M, Jemec GB. Pre-surgical high resolution ultrasound of facial basal cell carcinoma: correlation with histology. Cancer Imaging. 2008;8:163–72.

13. Uhara H, Hayashi K, Koga H, Saida T. Multiple hypersonographic spots in basal cell carcinoma. Dermatol Surg. 2007;33:1215–9.
14. Ekwueme DU, Guy G, Li C, Rim SH, Parelkar P, Chen SC. The health burden and economic costs of cutaneous melanoma mortality by race/ethnicity-United States, 2000 to 2006. J Am Acad Dermatol. 2011;6(S1):S133–43.
15. Reintgen DS, Vollmer R, Tso CY, Seigler HF. Prognosis for recurrent stage I malignant melanoma. Arch Surg. 1987;122:1338–42.
16. Nazarian LN, Alexander AA, Kurtz AB, Capuzzi Jr DM, Rawool NM, Gilbert KR, et al. Superficial melanoma metastases: appearances on gray-scale and color Doppler sonography. AJR Am J Roentgenol. 1998;170:459–63.
17. Netscher DT, Leong M, Orengo I, Yang D, Berg C, Krishnan B. Cutaneous malignancies: melanoma and nonmelanoma types. Plast Reconstr Surg. 2011;127:37e–56.
18. McKee P, Calonje E, Granter S. Melanoma. In: MacKee P Calonje E, Granter S. editors. Pathology of the skin with clinical correlations. 3rd ed. Philadelphia: Elsevier/Mosby; 2005. p. 1309–56.
19. Wortsman X. Sonography of the primary cutaneous melanoma: a review. Radiol Res Pract. 2012;2012:814396.
20. Tacke J, Haagen G, Horstein O, Huettinger G, Kiesewetter F, Schell H, et al. Clinical relevance of sonometry-derived tumour thickness in malignant melanoma—a statistical analysis. Br J Dermatol. 1995;132:209–14.
21. Guitera P, Li LX, Crotty K, Fitzgerald P, Mellenbergh R, Pellacani G, et al. Melanoma histological Breslow thickness predicted by 75-MHz ultrasonography. Br J Dermatol. 2008;159:364–9.
22. Hoffmann K, Jung J, el Gammal S, Altmeyer P. Malignant melanoma in 20-MHz B scan sonography. Dermatology. 1992;185:49–55.
23. Kaikaris V, Samsanavičius D, Maslauskas K, Rimdeika R, Valiukevičienė S, Makštienė J, et al. Measurement of melanoma thickness–comparison of two methods: ultrasound versus morphology. J Plast Reconstr Aesthet Surg. 2011;64:796–802.
24. Catalano O, Siani A. Cutaneous melanoma: role of ultrasound in the assessment of locoregional spread. Curr Probl Diagn Radiol. 2010;39:30–6.
25. Vilana R, Puig S, Sanchez M, Squarcia M, Lopez A, Castel T, et al. Preoperative assessment of cutaneous melanoma thickness using 10-MHz sonography. AJR Am J Roentgenol. 2009;193:639–43.
26. Music MM, Hertl K, Kadivec M, Pavlović MD, Hocevar M. Preoperative ultrasound with a 12–15 MHz linear probe reliably differentiates between melanoma thicker and thinner than 1 mm. J Eur Acad Dermatol Venereol. 2010;24:1105–8.
27. Lassau N, Mercier S, Koscielny S, Avril MF, Margulis A, Mamelle G, et al. Prognostic value of high-frequency sonography and color doppler sonography for the preoperative assessment of melanomas. AJR Am J Roentgenol. 1999;172:457–61.
28. Lassau N, Koscielny S, Avril MF, Margulis A, Duvillard P, De Baere T, et al. Prognostic value of angiogenesis evaluated with high-frequency and color Doppler sonography for preoperative assessment of melanomas. AJR Am J Roentgenol. 2002;178:1547–51.
29. Lassau N, Spatz A, Avril MF, Tardivon A, Margulis A, Mamelle G, et al. Value of high-frequency US for preoperative assessment of skin tumors. Radiographics. 1997;17:1559–65.
30. Voit C, Van Akkooi AC, Schäfer-Hesterberg G, Schoengen A, Kowalczyk K, Roewert JC, et al. Ultrasound morphology criteria predict metastatic disease of the sentinel nodes in patients with melanoma. J Clin Oncol. 2010;28:847–52.
31. Nazarian LN, Alexander AA, Rawool NM, Kurtz AB, Maguire HC, Mastrangelo MJ. Malignant melanoma: impact of superficial US on management. Radiology. 1996;199:273–7.
32. Catalano O, Voit C, Sandomenico F, Mandato Y, Petrillo M, Franco R, et al. Previously reported sonographic appearances of regional melanoma metastases are not likely due to necrosis. J Ultrasound Med. 2011;30:1041–9.
33. Tombesi P, Tassinari D, Sartori S. Contrast-enhanced ultrasound for characterizing lymph nodes with focal cortical thickening in patients with cutaneous melanoma. AJR Am J Roentgenol. 2011;197:W371.
34. Rubaltelli L, Beltrame V, Tregnaghi A, Scagliori E, Frigo AC, Stramare R. Contrast-enhanced ultrasound for characterizing lymph nodes with focal cortical thickening in patients with cutaneous melanoma. AJR Am J Roentgenol. 2011;196:W8–12.
35. Lassau N, Chami L, Chebil M, Benatsou B, Bidault S, Girard E, et al. Dynamic contrast-enhanced ultrasonography (DCE-US) and anti-angiogenic treatments. Discov Med. 2011;11:18–24.
36. Forsberg F, Ro RJ, Liu JB, Lipcan KJ, Potoczek M, Nazarian LN. Monitoring angiogenesis in human melanoma xenograft model using contrast-enhanced ultrasound imaging. Ultrason Imaging. 2008;30:237–46.
37. Goldberg BB, Merton DA, Liu JB, Forsberg F, Zhang K, Thakur M, et al. Contrast-enhanced ultrasound imaging of sentinel lymph nodes after peritumoral administration of Sonazoid in a melanoma tumor animal model. J Ultrasound Med. 2011;30:441–53.
38. Bhatia KS, Yuen EH, Cho CC, Tong CS, Lee YY, Ahuja ATA. Pilot study evaluating real-time shear wave ultrasound elastography of miscellaneous non-nodal neck masses in a routine head and neck ultrasound clinic. Ultrasound Med Biol. 2012;38:933–42.
39. Hinz T, Wenzel J, Schmid-Wendtner MH. Real-time tissue elastography: a helpful tool in the diagnosis of cutaneous melanoma? J Am Acad Dermatol. 2011;65:424–6.
40. Kirkpatrick SJ, Wang RK, Duncan DD, Kulesz-Martin M, Lee K. Imaging the mechanical stiffness of skin lesions by in vivo acousto-optical elastography. Opt Express. 2006;14:9770–9.
41. Rouffiac V, Duret JS, Péronneau P, Dehez N, Opolon P, Roche A, et al. Combination of HIFU therapy with contrast-enhanced sonography for quantitative assessment of therapeutic efficiency on tumor grafted mice. Ultrasound Med Biol. 2006;32:729–40.
42. Xing Y, Lu X, Pua EC, Zhong P. The effect of high intensity focused ultrasound treatment on metastases in a murine melanoma model. Biochem Biophys Res Commun. 2008;375:645–50.
43. Oliveira-Soares R, Viana I, Vale E, Soares-Almeida LM, Picoto A. Dermatofibrosarcoma protuberans: a clinicopathological study of 20 cases. J Eur Acad Dermatol Venereol. 2002;16:441–6.
44. Nouri K, Lodha R, Jimenez G, Robins P. Mohs micrographic surgery for dermatofibrosarcoma protuberans: University of Miami and NYU experience. Dermatol Surg. 2002;28:1060–4.
45. Thornton SL, Reid J, Papay FA, Vidimos AT. Childhood dermatofibrosarcoma protuberans: role of preoperative imaging. J Am Acad Dermatol. 2005;53:76–83.
46. Shin YR, Kim JY, Sung MS, Jung JH. Sonographic findings of dermatofibrosarcoma protuberans with pathologic correlation. J Ultrasound Med. 2008;27:269–74.
47. Donghi D, Kerl K, Dummer R, Schoenewolf N, Cozzio A. Cutaneous angiosarcoma: own experience over 13 years. Clinical features, disease course and immunohistochemical profile. J Eur Acad Dermatol Venereol. 2010;24:1230–4.
48. Wollina U, Hansel G, Schönlebe J, Averbeck M, Paasch U, Uhl J, et al. Cutaneous angiosarcoma is a rare aggressive malignant vascular tumour of the skin. J Eur Acad Dermatol Venereol. 2011;25:964–8.
49. Morgan MB, Swann M, Somach S, Eng W, Smoller B. Cutaneous angiosarcoma: a case series with prognostic correlation. J Am Acad Dermatol. 2004;50:867–74.
50. Kamo R, Ishii M. Histological differentiation, histogenesis and prognosis of cutaneous angiosarcoma. Osaka City Med J. 2011;57:31–44.
51. Costache M, Ene AM, Simionescu O, Sajin M. Histopathological diagnosis of cutaneous vascular sarcomas. Rom J Morphol Embryol. 2010;51:105–9.
52. Gasparetto TD, Marchiori E, Lourenço S, Zanetti G, Vianna AD, Santos AA, et al. Pulmonary involvement in Kaposi sarcoma: correlation between imaging and pathology. Orphanet J Rare Dis. 2009;4:18.

53. Restrepo CS, Ocazionez D. Kaposi's sarcoma: imaging overview. Semin Ultrasound CT MR. 2011;32:456–69.
54. Requena L, Requena C. Histopathology of the more common viral skin infections. Actas Dermosifiliogr. 2010;101:201–16.
55. Solivetti FM, Elia F, Latini A, Cota C, Cordiali-Fei P, Di Carlo A. AIDS-kaposi sarcoma and classic kaposi sarcoma: are different ultrasound patterns related to different variants? J Exp Clin Cancer Res. 2011;30:40.
56. Haddow LJ, Davies S, Buckingham S, Miller RF. Kaposi's sarcoma infiltrating skeletal muscle. Sex Transm Infect. 2002;78:464–5.
57. Bogner JR, Zietz C, Held M, Späthling S, Sandor P, Kronawitter U, et al. Ultrasound as a tool to evaluate remission of cutaneous Kaposi's sarcoma. AIDS. 1993;7:1081–5.
58. Duprat JP, Landman G, Salvajoli JV, Brechtbühl ER. A review of the epidemiology and treatment of Merkel cell carcinoma. Clinics (Sao Paulo). 2011;66:1817–23.
59. Nicolaidou E, Mikrova A, Antoniou C, Katsambas AD. Advances in Merkel cell carcinoma pathogenesis and management: a recently discovered virus, a new international consensus staging system and new diagnostic codes. Br J Dermatol. 2012;166:16–21.
60. Pileri Jr A, Patrizi A, Agostinelli C, Neri I, Sabattini E, Bacci F, et al. Primary cutaneous lymphomas: a reprisal. Semin Diagn Pathol. 2011;28:214–33.
61. Galper SL, Smith BD, Wilson LD. Diagnosis and management of mycosis fungoides. Oncology (Williston Park). 2010;24: 491–501.
62. McKee P, Calonje E, Granter S. Cutaneous lymphoproliferative diseases and related disorders. In: MacKee P Calonje E, Granter S, editors. Pathology of the skin with clinical correlations. 3rd ed. Philadelphia: Elsevier/Mosby; 2005. p. 1357–457.
63. Oztürk E, Sipahioglu S, Han U, Yücesoy C, Dilli A, Hekimoğlu B. Ultrasonography and MRI findings of cutaneous B-cell lymphoma, leg type. JBR-BTR. 2011;94:81–2.
64. Ushiki T, Nikkuni K, Higuchi T, Takai K. Multimodality imaging of subcutaneous panniculitis-like T-cell lymphoma. Intern Med. 2011;50:1265.